ASME Journal of Thermal Science and Engineering Applications
https://journaltool.asme.org/home/JournalDescriptions.cfm?JournalID=24&Journal=TSEA
Impact Factor = 1.544

Accepted January 29th 2021

SPECTRAL NUMERICAL STUDY OF ENTROPY GENERATION IN MAGNETO-CONVECTIVE VISCOELASTIC BIOFLUID FLOW THROUGH PORO-ELASTIC MEDIA WITH THERMAL RADIATION AND BUOYANCY EFFECTS

B. Mallikarjuna[1*], G. Gopi Krishna[2], J. Srinivas[3,] O. Anwar Bég[4] and Ali Kadir[4]

[1]*Department of Mathematics, BMS College of Engineering, Bangalore, Karnataka, India-560019.*
[2]*Department of Mathematics, Sri Venkateswara University, Tirupati, India.*
[3]*Department of Mathematics, National Institute of Technology Warangal, Warangal, India.*
[4]*Multi-Physical Engineering Sciences, Department of Aeronautical and Mechanical Engineering, School of Computing, Science and Engineering, Newton Building, The Crescent, Salford M54WT, UK*
**Corresponding Author: mallikarjunab.maths@bmsce.ac.in*

ABSTRACT:

Electromagnetic high-temperature therapy is popular in medical engineering treatments for various diseases include tissue damage ablation repair, hyperthermia and oncological illness diagnosis. The simulation of transport phenomena in such applications requires multi-physical models featuring magnetohydrodynamics, biorheology, heat transfer and deformable porous media. Motivated by investigating the fluid dynamics and thermodynamic optimization of such processes, in the present article a mathematical model is developed to study the combined influence of thermal buoyancy, magnetic field and thermal radiation on the entropy generation, momentum and heat transfer characteristics in electrically-conducting viscoelastic biofluid flow through a vertical deformable porous medium. Jefferys elastic-viscous model is deployed to simulate non-Newtonian characteristics of the biofluid. It is assumed that heat is generated within the fluid by both viscous and Darcy (porous matrix) dissipations. The governing equations for fluid velocity, solid displacement and temperature are formulated in a Cartesian coordinate system. The boundary value problem is normalized with appropriate transformations. The non-dimensional biofluid velocity, solid displacement and temperature equations with appropriate boundary conditions are solved computationally using a spectral method. Verification of accuracy is conducted via monitoring residuals of the solutions. Validation of solutions with Runge-Kutta shooting quadrature is included. The effects of Jeffrey viscoelastic parameter, viscous drag parameter, magnetic field parameter, radiation parameter and buoyancy parameter on flow velocity, solid displacement, temperature and entropy generation are depicted graphically and interpreted at length. Increasing magnetic field and drag parameters are found to reduce the field velocity, solid displacement, temperature and entropy production. Higher magnitudes of thermal radiation parameter retard the flow and decrease Nusselt number whereas they elevate solid displacement. Entropy production is enhanced with an increase in buoyancy parameter and volume fraction of the fluid. *The novelty of the work is the simulatenous inclusion of multiple thermophysical phenomena and the consideration of thermodynamic optimization in coupled thermal/fluid/elastic media.* The computations provide an insight into multi-physical transport in electromagnetic radiative tissue ablation therapy and a good benchmark for more advanced simulations.

Key words: *Deformable porous media; magnetohydrodynamics; thermal convection; electro-conductive viscoelastic fluids; radiative heat transfer; spectral computation; bio-magneto-thermal therapy.*

**** Corresponding Author: Email-*** *mallikarjuna.jntua@gmail.com, and mallikarjunab.maths@bmsce.ac.in*

1. INTRODUCTION

The study of fluid flow in undeformable (rigid) permeable media has been a very active research area embracing many branches of engineering and science. There are number of natural and industrial processes in which the medium is not rigid including geomaterials, biomaterials, insulation etc [1]. For these materials the forces which are exerted by the flow can cause substantial deformations of the medium. This deformation can, in turn, have a significant impact on the fluid flow itself if the properties of the material which govern the flow change with the deformation. The flow and deformation are coupled in deformable porous media and an analysis of the problem requires the simultaneous solution of the viscous flow and elastic deformation equations. Transport in poro-elastic media features in many applications including engineering seismology, geotechnics, biomechanics, energy dissipation systems etc. A popular approach in simulating deformable porous media is the *theory of mixtures* which has been lucidly described by Biot [2] in the context of geomechanics. Subsequently this approach has been adopted in biomechanics as it provides a good framework for modelling biological porous media including arterial wall permeability, articular cartilage, skin, pulmonary transport, bone etc. Mow *et al.* [3] presented an extensive review on mechanical and fluid transport properties of articular cartilage with consideration of the theory of mixtures. Lai *et al.* [4] discussed the deformation behaviour and swelling of articular cartilage. Barry *et al.* [5] investigated the unsteady flow of a Newtonian fluid through channel filled with deformable porous media. Sreenadh *et al.* [6, 7] developed mathematical models for multi-physical transport in deformable porous media with consideration of buoyancy and magnetic effects.

In numerous biological processes, heat transfer is present and may arise frequently as thermal conduction, convection or radiation. In these bio-thermal systems, energy losses are incurred which can cause disorder. Avoiding or controlling this energy loss in thermal processes has gained much interest among researchers in recent years. Analysis of entropy generation is a powerful tool by which one can minimize the energy wastage or utilize it in an optimum way to improve the system performance. Bejan [8] introduced the entropy generation minimization (EGM) approach, initially for industrial thermal systems. Since generically thermal processes are inherently irreversible, this leads to continuous entropy generation, which eliminates the exergy (useful energy or available energy for work) of a system via different modes of heat transfer (thermal conduction, convection and radiation) .

In biological systems other phenomena may also contribute to the entropy production including electrical fields (due to ions), magnetic fields (associated with iron in the haemoglobin molecule), viscosity (fluid friction), magnetic field, thermal buoyancy, species buoyancy etc. Minimization in the loss of exergy in any system is desirable since it permits optimal usage of the energy situation with minimum irreversibilities. This optimum condition can be assessed via entropy generation minimization (EGM) . A number of diverse problems in medical engineering sciences have been studied with this technique in recent years. Entropy generation minimization (EGM) provides an enhanced understanding of thermodynamic efficiency of biological systems and can aid in optimizing numerous biomedical processes including cryo-preservation [9], cell dynamics [10], peripheral neuropathy [11], novel bio-thermodynamic anti-cancer strategies [12], vascular blood flows [13], reactive hyperthermia for spinal cord injury treatment [14] and extra-corporeal blood flow control [15]. It utilizes the second law of thermodynamics to enable a more refined appraisal of heat transfer and mitigation of losses. Computational studies of entropy generation in porous media have been communicated by for example Vasu *et al.* [16] who considered a Darcian porous medium and computed thermal dispersion effects on entropy generation rates with a Chebyshev spectral collocation method). Srinivas and Raman Murthy [17] investigated analytically the microstructural fluid flow in dual porous regimes in a horizontal channel. Akbar *et al.* [18] observing that entropy generation rate is enhanced with both Darcy and Brinkman number (ratio of direct heat conduction from the wall surface to the viscous heat generated by shear in the boundary layer). They also showed that Bejan number (ratio of heat transfer irreversibility to total irreversibility due to heat transfer and fluid friction) is elevated with both increasing Brinkman number and Darcy number. Datta *et al.* [19] studied the entropy generation with thermal convection in a square enclosure containing a porous medium , computing heatlines, Nusselt number, streamlines, entropy generation and irreversibility production in the enclosure. Rashidi *et al.* [20] studied free convection and entropy generation of nanofluid flow in a vertical cylinder under heterogeneous heat flux.

Magnetohydrodynamics (MHD) is also an active area of modern biomedical engineering sciences. It involves the interaction of applied magnetic fields with electrically-conducting flows. Blood for example is electrically-conducting owing to the presence of haemoglobin in the iron molecule and plasma and other physiological liquids contain

significant levels of ions [21]. Other physiological fluids which respond to magnetic fields are synovial lubricants, plasma, occular fluids etc. The imposition of external (extra-corporeal) magnetic fields is also beneficial in pain therapy since it successfully controls flow. To properly quantify the effectiveness of magnetic therapy, for example, magnetic drug targeting for different cancerous diseases, it is important to develop realistic magnetohydrodynamic physiological flow models which properly simulate the influence of magnetic fields on transport phenomena (flow, heat and mass transfer). The relative contribution of viscous hydrodynamic force and Lorentz magnetic drag force is usually critical in such simulations and influences entropy generation rates. Several investigations have therefore considered entropy generation minimization in biological magneto-thermal fluid dynamics. Bég *et al.* [22] computed Bejan numbers and entropy generation rates in magnetized biofluid transport from a rotating disk using a homotopy technique. Khan *et al.* [23] analysed the entropy generation rate in thin film reactive mixed convection magnetohydrodynamic viscoelastic nanofluid bioconvection in a Darcian porous regime. Radiative heat transfer with entropy generation has also stimulated some interest. Ramana Murthy *et al.* [24] studied thermal radiation effects on entropy generation in channel flow and heat transfer in dual immiscible non-Newtonian Stokes' couple stress fluids. They showed that entropy production is reduced by thermal radiation whereas it is enhanced with viscous dissipation. Srinivas *et al.* [25] computed porous media drag and radiative effects on entropy generation in micropolar natural convection flow. Jamalabadi *et al.* [26] studied combined viscous dissipation and radiative effects on entropy generation non-Newtonian power-law convection from an axi-symmetric stretching sheet. Shukla *et al.* [27] obtained finite element solutions for entropy generation characteristics in radiative stagnation-point nanofluid flow under both electrical and magnetic fields. Muthukumar *et al.* [28] investigated on MHD convective flow of a nanofluid in a lid driven porous enclosure under the influence of thermal radiation with non-uniform thermal vertical walls. Sheikholeslami *et al.* [29] used finite element method to compute the solutions of the developed mathematical model on MHD free convective-radiative flow of a nanofluid inside a corrugated annulus.

Liquids exhibiting characteristics which are both solid- and fluid-like are categorized as viscoelastic fluids. Such fluids are classified as *non-Newtonian* and possess time-dependent or rate-sensitive stress-strain relations. Many physiological liquids behave as

viscoelastic fluids. Pertinent examples include blood [30] which contains numerous suspensions such as non-protein hormones, lipids, proteins, nutrients, electrolytes, gases, erythrocytes, leukocytes etc. Other examples are synovial fluid in the human knee [31], gels in the human eye [32], submucosal injection materials (SIMs) in early-stage gastrointestinal neoplasm treatment [33], sub-mandilar saliva [34] and blood-plasma [35]. The inadequacy of the Navier-Stokes equations in simulating such fluids has motivated researchers to deploy an extensive spectrum of viscoelastic fluid models which feature different material characteristics including relaxation times, viscosity, elasticity, retardation, normal stress differences etc. The heat-conducting nature of blood and other biological and industrial liquids has also attracted interest from a thermodynamic optimization viewpoint. Entropy in chemically-reacting third grade Reiner-Rivlin fluids has been considered by Adesanya *et al.* [36]. Kumar *et al.* [37] conducted an entropy generation minimization and Bejan heat line visualization analysis of time-dependent free convection flow of a second grade elastic-viscous fluid external to a cylindrical geometry with the Crank-Nicolson finite difference method. They showed that an increase in viscoelasticity, viscosity and Grashof number reduces entropy generation. Among the most versatile nonlinear viscoelastic hydrodynamic models developed is the *Jeffrey fluid model*. This non-Newtonian model represents biophysical fluids reasonably well and features three constants i.e. viscosity at zero shear rate, and two time-related material parameter constants . A number of studies have reported on the suitability of the Jeffery rheological model for biological hydrodynamics including Vajravelu *et al.* [38] and Tripathi and Bég [39]. Magnetohydrodynamic thermal therapy of biological viscoelastic fluent media has also been explored extensively and relevant examples include structural modification of synovial fluids in orthopaedics [40], affinity-based magnetic purification of blood plasma [41], magnetized pharmaco-dynamics [42] and treatment of ocular and cochlear disorders with magneto-acoustics [43]. Several mathematical studies have also appeared focused on biological magnetothermal flow with the electrically-conducting Jeffrey model. Manzoor *et al*. [44] employed the Adomian decomposition method (ADM) to investigate hydromagnetic ciliated propulsion of Jeffrey's viscoelastic fluids with heat transfer in a porous medium channel with viscous dissipation effects, observing that the Jefferys parameter (stress relaxation time to retardation time ratio) substantially modifies momentum and thermal characteristics. Ramesh *et al.* [45] studied theoretically the magnetohydrodynamic (MHD) peristaltic pumping of viscoelastic two-phase blood in a deformable channel, noting that higher values of Jefferys viscoelastic parameter

retard the fluid phase flow, accelerate the particle phase flow, decrease axial pressure gradient, enhance pressure difference in the augmented pumping region and reduce pressure difference in the pumping region.

In many biological systems and medical devices, as noted earlier the medium is poro-elastic. It undergoes elastic deformation and simultaneously permits fluid percolation. Although some investigations have been communicated on entropy generation in media with deformable boundaries, the simulation of entropy generation in deformable porous media has emerged more recently. Important studies in this regard include Gopi Krishna *et al.* [46] who studied Casson viscoplastic heat transfer with entropy generation in a vertical porous medium channel. Gopi Krishna *et al.* [47] further investigated the entropy generation in viscous flow in an inclined deformable porous layer containing a heat source bound by rigid plates, noting that fluid velocity, temperature and entropy generation decrease with increasing viscous drag whereas solid displacement increases with increasing viscous drag. They further observed *that* volumetric flow rate is greater for undeformable (rigid) porous media as compared with deformable porous media.

In the present article, a numerical study is conducted to elucidate the collective effects of thermal buoyancy, magnetic field and thermal radiation on the flow, heat transfer and entropy generation in magnetized viscoelastic Jeffrey's biofluid in a vertical deformable porous medium which is absent in the technical literature. The emerging non-dimensional boundary value problem is solved with the robust, accurate, convergent iterative computational spectral quasilinearization method (SQM) [45]. Validation of solutions with Runge-Kutta shooting quadrature [46] is included. The effects of Jeffrey viscoelastic parameter, viscous drag parameter, magnetic field parameter, radiation parameter and buoyancy parameter on flow velocity, solid displacement and temperature are depicted graphically. The simulations are relevant to bio-magnetic high temperature therapy processes and to the authors' knowledge constitute a novel contribution to the literature. In biomagnetic therapy magnetic fields generate thermal effects in solid/fluid composite biomaterials in the human body. The interstitial fluid is often non-Newtonian, therefore a rheological model with magnetic body force terms must be employed since the ionic nature of biofluids makes them electrically conducting. This is the novelty of the work - a much more comprehensive multi-physical formulation is given then previously published anywhere in the literature- many effects are considered simultaneously, which have not been reported

before in tissue electriomagnetic ablation therapy. These results will therefore benefit understanding in articular carteilage, perfused tissue and other areas.

2. MODEL FOR MAGNETO-VISCOELASTIC TRANSPORT IN DEFORMABLE MEDIUM

The regime under consideration comprises the steady, fully-developed, free convective-radiative flow of an electrically-conducting Jeffrey viscoelastic physiological fluid through a vertical deformable porous medium bound by rigid walls. The porous material is elastic and deformable and is modelled as a continuous binary mixture of solid and fluid phases where each point in the mixture is occupied continuously by both the fluid and solid. The porous matrix is saturated with viscoelastic biofluid. Darcy's law is assumed and the medium is considered as isotropic and homogenous. Tortuosity effects are neglected. The X -axis is taken along the middle of the channel geometry and the Y -axis is orientated perpendicular to the X -axis. A uniform static magnetic field is applied along the Y -axis. The plates of the channel are maintained at constant and uniform temperature T_1 respectively. Magnetic Reynolds number is negligibly small and therefore magnetic induction effects are negated. It is also assumed that applied or polarized voltage is neglected so that no energy is added or extracted from the fluid by electrical means. The biofluid is considered to be a gray, absorbing-emitting but non-scattering medium and the Rosseland approximation is used to describe the radiative heat flux which also acts transverse to the plates. The radiative heat flux in the *X*-direction is considered negligible in comparison with that in the *Y*-direction. Optical density of the fluent medium is considered to be high for which the Rosseland approximation is valid. A constant pressure gradient $\frac{\partial P}{\partial X}$ is applied to produce an axially upward directed flow. The channel width is *2h*. The physical regime is illustrated in **Fig. 1**. The constitutive equations for an incompressible Jeffrey fluid [35, 36] flow are $\bar{\bar{T}} = -\bar{P}\bar{\bar{I}} + \bar{\bar{s}}$, where $\bar{\bar{T}}$ and $\bar{\bar{s}} = \frac{\mu}{1+\lambda_1}\left(\dot{\bar{\gamma}} + \lambda_2 \ddot{\bar{\gamma}}\right)$ are the Cauchy stress tensor and extra stress tensor respectively, $\bar{P}$ is the pressure, $\bar{\bar{I}}$ is the identity tensor, λ_1 is the ratio of relaxation to retardation time (Jeffrey elastic-viscous parameter), λ_2 is the retardation time, $\dot{\gamma} = \nabla\bar{q} + \left(\nabla\bar{q}\right)^T$ is shear rate and dots over the quantities indicate differentiation with respect to time i.e. $\dot{\gamma} = \frac{d\dot{\gamma}}{dt} = \frac{\partial\dot{\gamma}}{\partial t} + \left(\bar{q}\cdot\nabla\right)\dot{\gamma}$ where $\frac{d}{dt}$ is the material derivative and $\bar{q}$ is the fluid velocity vector.

Incorporating the appropriate terms from the Jeffrey model, under the above assumptions, the governing equations extending the Newtonian model in [47] assume the form:

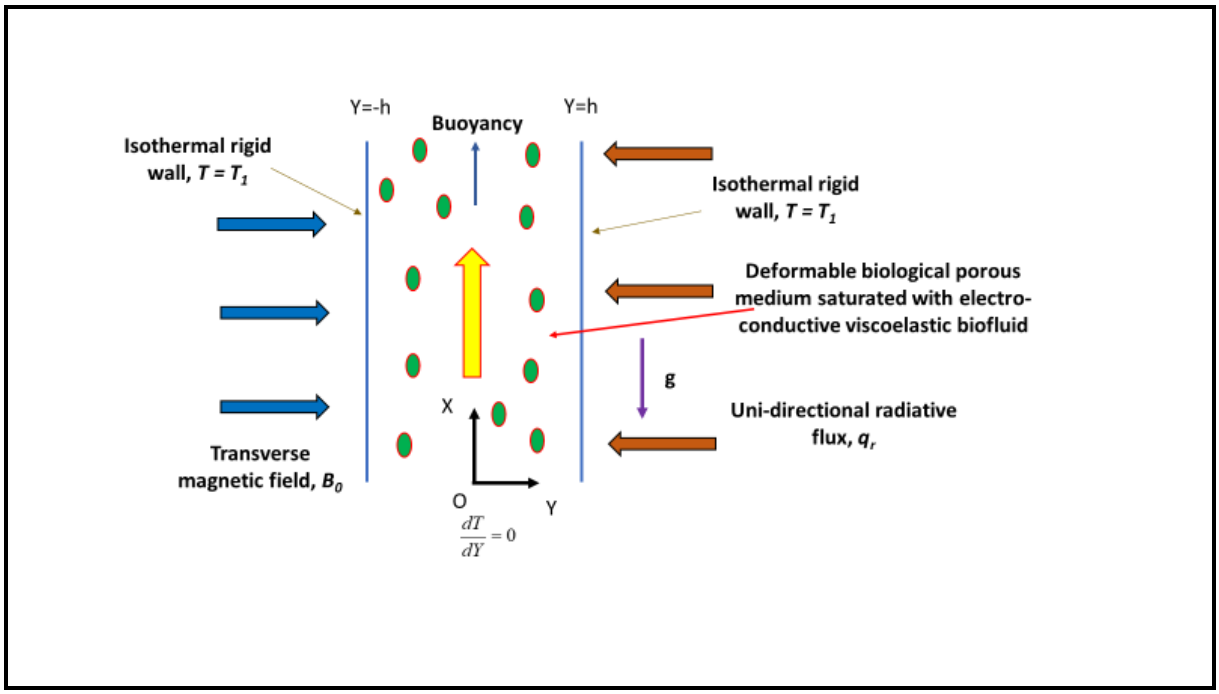

Fig. 1 Physical model of magnetic heat transfer in viscoelastic-saturated deformable porous medium

$$\mu\frac{\partial^2 U}{\partial Y^2}-(1-\phi)\frac{\partial P}{\partial X}+KV=0 \tag{1}$$

$$\frac{2\mu_a}{1+\lambda_1}\frac{\partial^2 V}{\partial Y^2}-\phi\frac{\partial P}{\partial X}-KV-\sigma B_0^2 V+\rho g\beta\left(T-T_0\right)=0 \tag{2}$$

$$\frac{K_0}{\rho c_p}\frac{\partial^2 T}{\partial Y^2}+\frac{2\mu_a}{\left(1+\lambda_1\right)\rho c_p}\left(\frac{\partial V}{\partial Y}\right)^2-\frac{1}{\rho c_p}\frac{\partial q_r}{\partial Y}=0 \tag{3}$$

where μ is the apparent (dynamic) viscosity of the fluid in the porous material, U is the solid displacement, ϕ is porous medium volume fraction, $\frac{\partial P}{\partial X}$ is the axial pressure gradient K is the porous media drag coefficient, V is the flow velocity, μ_a is the Lamé constant, λ_1 is ratio of relaxation and retardation time, σ is biofluid electrical conductivity, B_o is applied magnetic field, ρ is the density of the biofluid, β is the coefficient of thermal expansion, T is biofluid temperature, T_o is an arbitrary temperature, K_o is thermal conductivity, c_p is isobaric

specific heat capacity, q_r is radiative flux. The system is symmetrical about the channel centreline. The boundary conditions at the channel centre-line and the right hand plate are:

$$\frac{dU}{dY}=0,\ \frac{dV}{dY}=0,\ \frac{dT}{dY}=0 \text{ at } Y=0 \text{ (Centre line)}$$

$$U=0,\ V=0,\ T=T_1 \text{ at } Y=h \text{ (Right hand side plate)} \tag{4}$$

Introducing the following dimensionless variables for transverse coordinate, axial coordinate, fluid velocity, solid displacement, temperature and pressure, respectively:

$$y=\frac{Y}{h},\ x=\frac{X}{h},\ v=\frac{2\mu_a V}{\rho g\beta h(T_1-T_0)},\ u=\frac{\mu U}{\rho g\beta h^2(T_1-T_0)},\ \theta=\frac{T-T_0}{T_1-T_0},\ p=\frac{P}{\rho g\beta h(T_1-T_0)} \tag{5}$$

In view of the above dimensionless variables, the governing elastic equilibrium and momentum conservation equations (1)-(2) emerge as:

$$\frac{d^2u}{dy^2}-(1-\phi)\frac{dp}{dx}+\delta v=0 \tag{6}$$

$$\frac{1}{(1+\lambda_1)}\frac{d^2v}{dy^2}-\phi\frac{dp}{dx}-\delta v-Mv+\theta=0 \tag{7}$$

where u is the non-dimensional solid displacement, v is the non-dimensional flow velocity in the deformable porous layer, ϕ is the volume fraction of the fluid, $\delta = Kh/(2\mu_a)$ is viscous drag parameter (Darcian impedance parameter), $M=\sqrt{\frac{\sigma B_0^2 h^2}{2\mu_a}}$ is the magnetic body force parameter and θ is non-dimensional temperature. According to Rosseland's diffusion approximation [48], the radiative heat flux (q_r) term can be written as:

$$q_r=-\frac{4}{3}\frac{\sigma^*}{k^*}\frac{\partial T^4}{\partial Y} \tag{8}$$

Here σ* and k* denote the Stefan-Boltzmann constant and mean absorption coefficient respectively. The Rosseland model retains reasonable accuracy for optically-thick media wherein thermal radiation propagates a limited distance prior to encountering scattering or absorption. The refractive index of the biofluid is assumed to be constant, intensity within the fluid is nearly isotropic and uniform, and furthermore wavelength regions exist where the

optical thickness is generally in excess of five. It is assumed that the temperature differences are small within the flow so that the quartic *non-linear* temperature term, T^4 can be expressed as a *linear* function using Taylor's series expansion about T_1 i.e. $T^4 = 4T_1^3 T - 3T_1^4$. Substituting this in eqn. (8), we obtain

$$\frac{\partial q_r}{\partial Y} = -\frac{16}{3}\frac{\sigma^* T_1^3}{k^*}\frac{\partial^2 T}{\partial Y^2} \tag{9}$$

Again substituting eqn. (9) in eqn. (3) and using the afore-mentioned dimensionless variables (5), we obtain:

$$\left(1+\frac{4}{3}R\right)\frac{d^2\theta}{dy^2} + \frac{N}{1+\lambda_1}\left(\frac{dv}{dy}\right)^2 + N\delta v^2 = 0 \tag{10}$$

Here $R = \frac{4\sigma^* T_1^3}{k^*}$ is the thermal radiation-conduction parameter, $N = \frac{\rho^2 g^2 \beta^4 h^4 (T_1 - T_0)}{2\mu_a k_0}$ is the thermal buoyancy parameter, and all other parameters have been defined earlier. The associated boundary conditions emerge as:

$$\frac{du}{dy} = \frac{dv}{dy} = \frac{d\theta}{dy} = 0 \text{ at } y = 0 \qquad \text{(channel centreline)} \tag{11}$$

$$u = 0, v = 0, \theta = 1 \text{ at } y = 1 \qquad \text{(right hand plate)} \tag{12}$$

3. SPECTRAL QUASI-LINEARIZATION METHOD (SQM) NUMERICAL SOLUTION

The set of non-linear coupled eqns. (6), (7) and (10) with boundary conditions Eq. (11) and Eq. (12) are solved numerically using the Spectral Quasi-Linearization Method (SQM). This method combines the exceptional accuracy of spectral collocation [49] with the traditional Bellman-Kalaba quasi-linearization method (QLM) yielding enhanced stability and accuracy. SQM has been utilized extensively in recent years in many diverse areas of engineering sciences including rocket propulsion [50], geological convection [51], bioheat transfer in tissue [52], electrodynamic propulsion [53] and biomagnetic hemodynamics [53]. The first step intrinsic to this approach is the linearization of the governing differential equations i.e. Eqns. (8)-(11) by QLM, following Bellman and Kalaba [45]. Next applying the QLM to Eqns. (6), (7) and (10) by assuming the approximate solutions, u_r, v_r and θ_r of solid displacement, velocity field and temperature field respectively, we get:

$$a_{1,1}^{2}u_{r+1}'' + a_{1,1}^{1}u_{r+1}' + a_{1,1}^{0}u_{r+1} + a_{1,2}^{0}v_{r+1} = R_1 \tag{13}$$

$$a_{2,2}^{2}v_{r+1}'' + a_{2,2}^{0}v_{r+1} + a_{2,3}\theta_{r+1} = R_2 \tag{14}$$

$$a_{3,3}^{2}\theta_{r+1}'' + a_{3,2}^{1}v_{r+1}' = R_3 \tag{15}$$

The boundary conditions become

$$\left.\begin{aligned} u_{r+1}' = v_{r+1}' = \theta_{r+1}' = 0 \ \text{ at } \ y = 0, \\ u_{r+1} = v_{r+1} = 0, \ \theta_{r+1} = 1 \text{at } \ y = 1 \end{aligned}\right\} \tag{16}$$

Here the featured coefficients in Eqns. (13)-(15) are defined as follows:

$$a_{1,1}^{2} = 1, a_{1,1}^{1} = 0, a_{1,1}^{0} = 0, a_{1,2}^{0} = \delta$$

$$a_{2,2}^{2} = 1, a_{2,2}^{0} = -(1+\lambda_1)\left(\delta + M^2\right), a_{2,3}^{0} = (1+\lambda_1)$$

$$a_{3,3}^{2} = 1 + \frac{4R}{3}, a_{3,2}^{1} = \frac{N}{(1+\lambda_1)}2v_r', a_{3,2}^{0} = N\delta 2v_r$$

$$R_1 = \left(1-\phi\right)P, \ R_2 = \phi(1+\lambda_1)P \text{ and } R_3 = \frac{N}{(1+\lambda_1)}\left(v_r'\right)^2 + N\delta v_r^2 \tag{17}$$

To compute the solutions of Eqns. (13)-(15) under boundary conditions Eq. (16) at the $\left(r+1\right)^{th}$ iteration, field variables are selected at the r^{th} position as $u_r = 0, v_r = 0, \theta_r = y$; satisfying the boundary conditions. Now according to the spectral method, the domain $y \in [0,1]$ is first transformed (mapped) onto $z \in [-1, 1]$ using the transformation, $\xi = \frac{1}{2}\left(z+1\right)$. Next the Chebyshev Gauss-Lobatto points are selected based on:

$$z_j = \cos\left(\frac{\pi j}{n}\right), \ \ j = 0(1)n, \tag{18}$$

Here n represents the number of collocation points. The field variables u_r, v_r and θ_r are approximated in terms of Lagrange polynomials (basis functions) at $N+1$ Gauss-Lobatto points, as, respectively:

$$u(\xi) = \sum_{j=0}^{n} \psi_j(\xi) u_j, \tag{19}$$

$$v(\xi) = \sum_{j=0}^{n} \psi_j(\xi) v_j \tag{20}$$

$$\theta(\xi) = \sum_{j=0}^{n} \psi_j(\xi) \theta_j \,. \tag{21}$$

Next the derivatives with respect to the basis functions about the collocation points are obtained (see Trefthen [49]) as:

$$D(\ ) = 2 \sum_{j=0}^{n} \psi_j'(\xi_i)(\ )_j \tag{22}$$

Eqns (13) - (15) with conditions Eq. (16) are discretized in terms of *Lagrangian polynomials* about these collocation points. This effectively leads to the following matrix system of equations in the form $AX = R$, where:

$$A = \begin{bmatrix} B_{11} & B_{12} & B_{13} \\ B_{21} & B_{22} & B_{23} \\ B_{31} & B_{32} & B_{33} \end{bmatrix}, X = \begin{bmatrix} u_{r+1} \\ v_{r+1} \\ \theta_{r+1} \end{bmatrix}, R = \begin{bmatrix} R_1 \\ R_2 \\ R_3 \end{bmatrix} \tag{23}$$

Here the following definitions apply:

$$B_{11} = diag(a_{1,1}^2) D^2, B_{12} = diag(a_{1,2}^0) I, B_{13} = O \tag{24}$$

$$B_{21} = O, B_{22} = diag(a_{2,2}^2) D^2 + diag(a_{2,2}^0) I, B_{23} = diag(a_{2,3}^0) I \tag{25}$$

$$B_{31} = O, B_{32} = diag(a_{3,2}^1) D, B_{33} = diag(a_{3,3}^2) D^2 \tag{26}$$

In Eqns. (24)-(26), D is the Chebyshev differentiation matrix, I is the Identity matrix of order N+1 and O is the zero matrix of order N+1. The boundary conditions are imposed in the matrices as follows:

$$B_{11}(n+1,:)=0, B_{11}(n+1,:)=D(n+1,:); B_{12}(n+1,:)=0;\ B_{13}(n+1,:)=0; R_1(n+1)=0;$$
$$B_{11}(1,:)=0; B_{11}(1,1)=1; B_{12}(1,:)=0; B_{13}(1,:)=0; R_1(1)=0; \quad (27)$$

$$B_{21}(n+1,:)=0; B_{22}(n+1,:)=0; B_{22}(n+1,:)=D(n+1,:); B_{23}(n+1,:)=0; R_2(n+1)=0;$$
$$B_{21}(1,:)=0; B_{22}(1,:)=0; B_{22}(1,1)=1; B_{23}(1,:)=0; R_2(1)=0; \quad (28)$$

$$B_{31}(n+1,:)=0; B_{32}(n+1,:)=0; B_{33}(n+1,:)=D(n+1,:); R_3(n+1)=0;$$
$$B_{31}(1,:)=0; B_{32}(1,:)=0; B_{33}(1,:)=0; B_{33}(1,1)=1; R_3(1)=1; \quad (29)$$

This system of equations can be solved by using the pseudo-inverse operator available in MATLAB®. In order to check the accuracy of the results, residuals of the solutions have been presented through Figs. (2)-(4). From these figures, it is perceived that solid displacement (u) and fluid velocity (v) results are obtained to an accuracy of 10^{-10} and θ to 10^{-9} accuracy. Convergence and accuracy of the solutions is therefore attained comfortably .

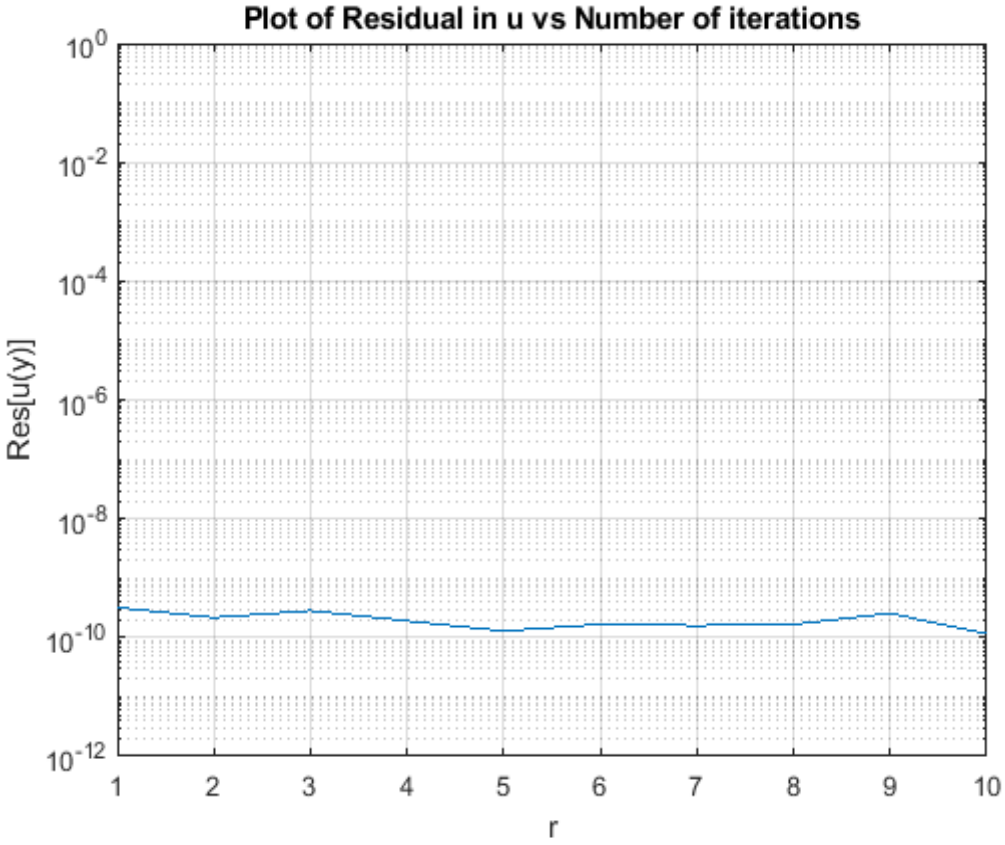

Figure 2: Residual of u for 10 iterations with *n=40* collocation points

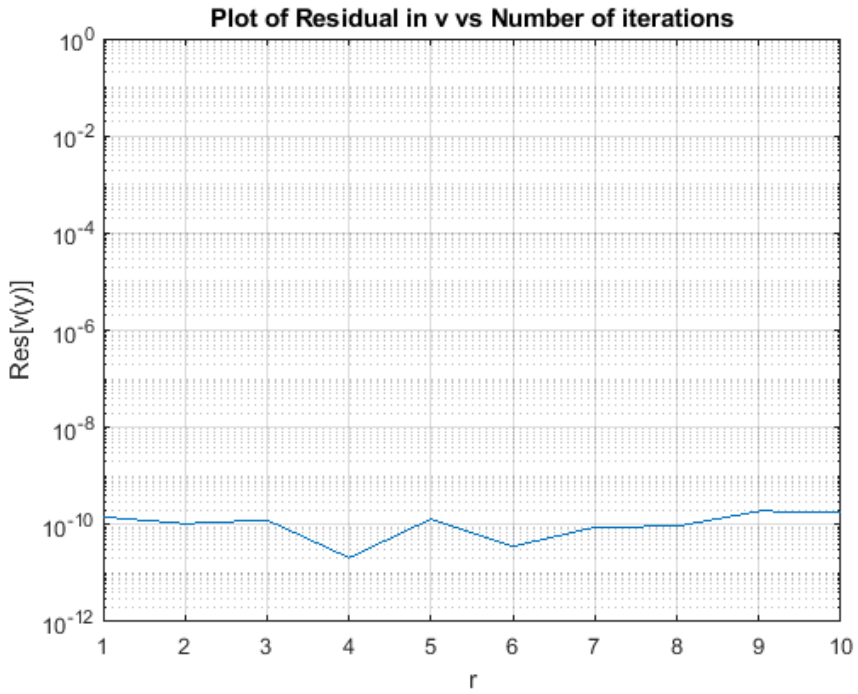

Figure 3: Residual of v for 10 iterations with *n=40* collocation points

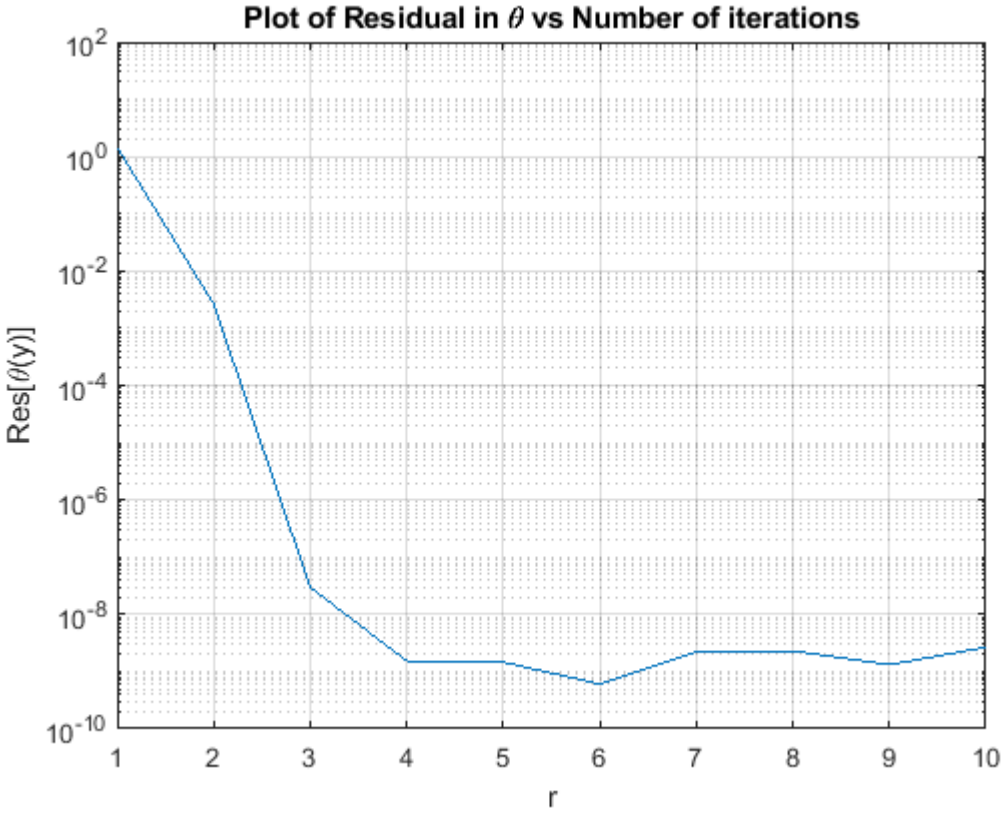

Figure 4: Residual of θ for 10 iterations with *n=40* collocation points

Further validation of the SQM solutions is confirmed via comparison with another numerical method i.e. shooting quadrature technique (see Mallikarjuna *et al.* [55] and Srinivasacharya *et al.* [56]). These are presented in Section 5.

4. ENTROPY GENERATION ANALYSIS

In almost all thermodynamic processes, avoiding energy wastage is of great importance, since most energy is dissipated as heat in the system. Bejan's entropy generation minimization (EGM) approach offers a practicable mechanism for optimizing energy usage which is critical in industrial and medical applications. Volumetric rate of entropy generation [57], $\left(E_G\right)\left(W/m^3K\right)$, based on the second law of thermodynamics for a deformable porous medium saturated with viscoelastic field with thermal radiation and magnetic field effects, takes the form:

$$E_G=\frac{k_0}{T_0^2}\left[\left(\frac{\partial T}{\partial Y}\right)^2+\frac{16}{3}\frac{\sigma^* T_1^2}{kk^*}\left(\frac{\partial T}{\partial Y}\right)^2\right]+\frac{2\mu_a}{T_0\left(1+\lambda_1\right)}\left(\frac{\partial V}{\partial Y}\right)^2+\frac{\sigma B_0^2}{T_0}V^2 \tag{30}$$

The first and second terms in the square brackets on the RHS are associated respectively with *thermal conduction* and thermal *radiative heat transfer*, the next term is due to *viscous dissipation* and the last term is due to magnetic body force. In dimensionless form, the entropy generation number can be determined using:

$$N_s=\frac{T_0^2h^2}{k_0\left(T_1-T_0\right)}E_G \tag{31}$$

Using variables defined earlier, the non-dimensional version of Eqn. (31), emerges as:

$$N_s=\left[1+\frac{4}{3}R\right]\left(\frac{d\theta}{dy}\right)^2+\frac{N}{\Omega}\left[\left(\frac{dv}{dy}\right)^2+Mv^2\right] \tag{32}$$

Here $\Omega=\left(T_1-T_0\right)/T_0$ is the dimensionless temperature difference and all other parameters have been defined previously. It is also noteworthy that entropy generation analysis (specifically the evaluation of the irreversibility distribution) can be conducted with the *Bejan*

number which is defined for the current model as the ratio of irreversibility due to radiative heat transfer to the total heat irreversibility due to radiative heat transfer, fluid friction, and magnetic body force, viz:

$$Be = \frac{\left(1+\frac{4}{3}R\right)\left(\frac{d\theta}{dy}\right)^2}{\left[1+\frac{4}{3}R\right]\left(\frac{d\theta}{dy}\right)^2 + \frac{N}{\Omega}\left[\left(\frac{dv}{dy}\right)^2 + Mv^2\right]} \tag{33}$$

However in the present simulations attention is focused on the entropy generation rates which are generally inversely proportional to the Bejan number. Further, it is apparent from Eq. (33) that the Bejan number (Be) values range from 0 to 1 (also see the discussion in Ref. [58]). The value of $Be = 0$ signifies the case of domination of irreversibility due to fluid friction and magnetic force over irreversibility due to thermal-radiative-conduction. The value of $Be = 1$ represents the case of domination of irreversibility due to thermal-radiative-conduction over the irreversibility due to fluid friction. Finally, the two irreversibility mechanisms contribute equally when $Be = 0.5$.

5. NUMERICAL RESULTS AND DISCUSSION:

Extensive computations have been performed and solutions are presented graphically in **Figs. 5-23** for fluid velocity (v), solid displacement (u) and temperature distribution (θ) with variation in key parameters. Default values of parameters are prescribed as follows unless otherwise stated: pressure gradient parameter $P = -1$, porous medium volume fraction $\phi = 0.6$, viscous drag parameter $\delta = 1$, radiation-conduction parameter $R = 1$, Jeffery viscoelastic parameter $\lambda_1 = 0.2$, magnetic parameter $M = 1$ and thermal buoyancy parameter $N = 1$. Physically these values imply negative pressure, high porosity, weak drag, equivalence of radiation and conduction heat transfer modes, weak viscoelasticity, equivalence of Hartmann magnetic drag and viscous hydrodynamic force and equivalence of thermal buoyancy and viscous hydrodynamic force, respectively. In addition to the

fundamental variables u,v,θ and entropy generation rate, N_S, it is also useful to study momentum and heat transfer characteristics at the channel wall (plate). Non-dimensional shear stress (skin friction), τ, is defined as:

$$\tau = [dv/dy]_{y=1} \quad (34)$$

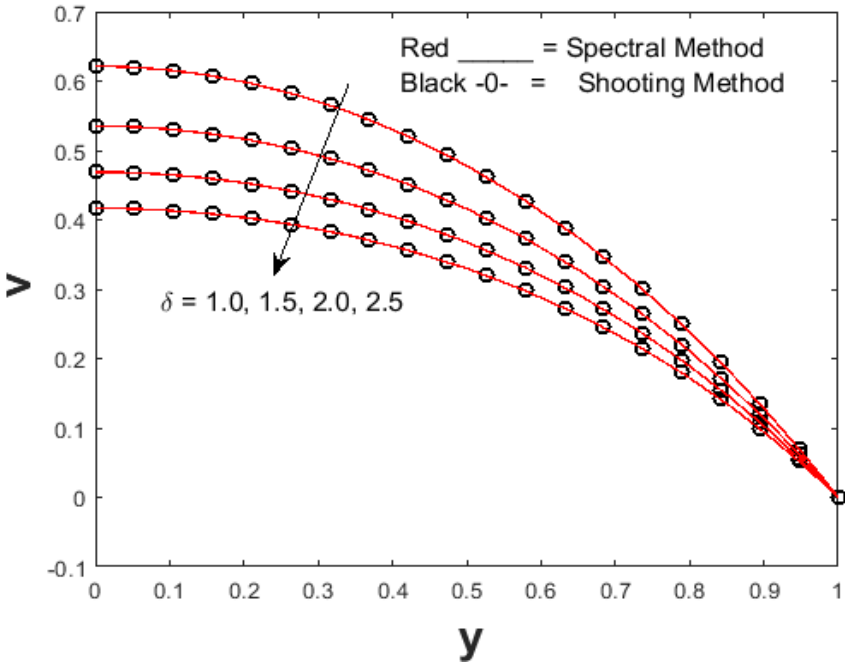

Figure 5: Velocity profiles for different values of δ

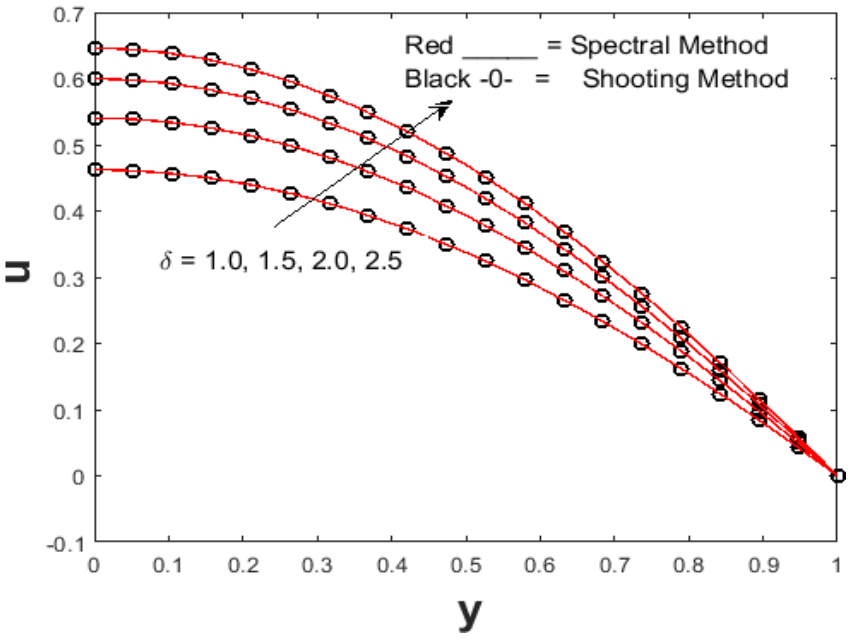

Figure 6: Displacement profiles for different values of δ

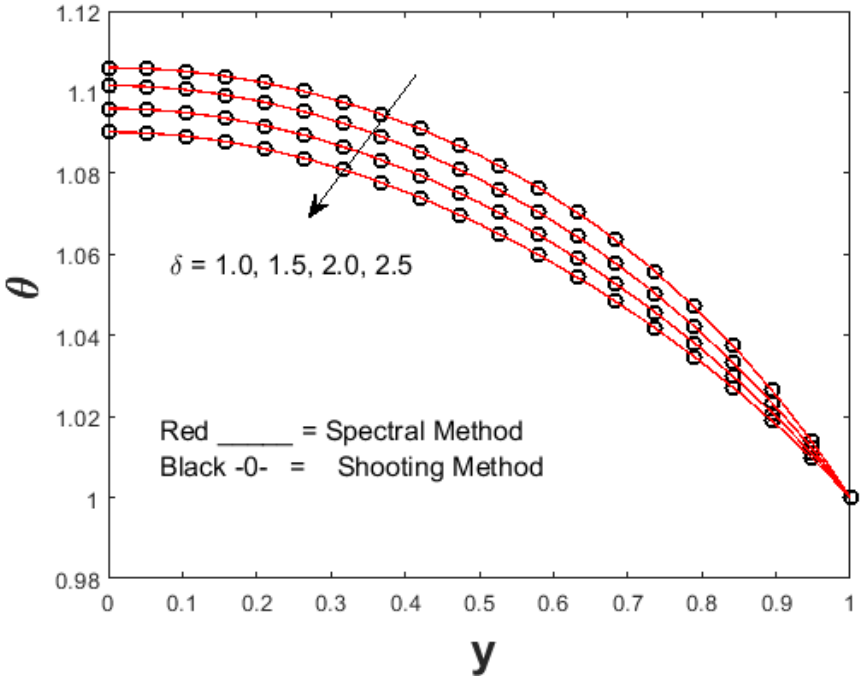

Figure 7: Temperature profiles for different values of δ

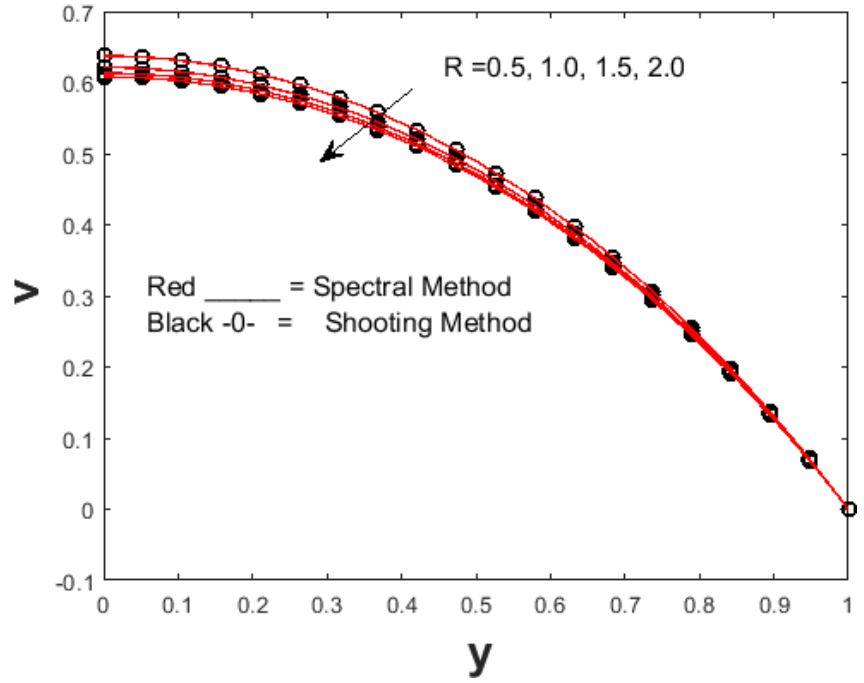

Figure 8: Velocity profiles for different values of R

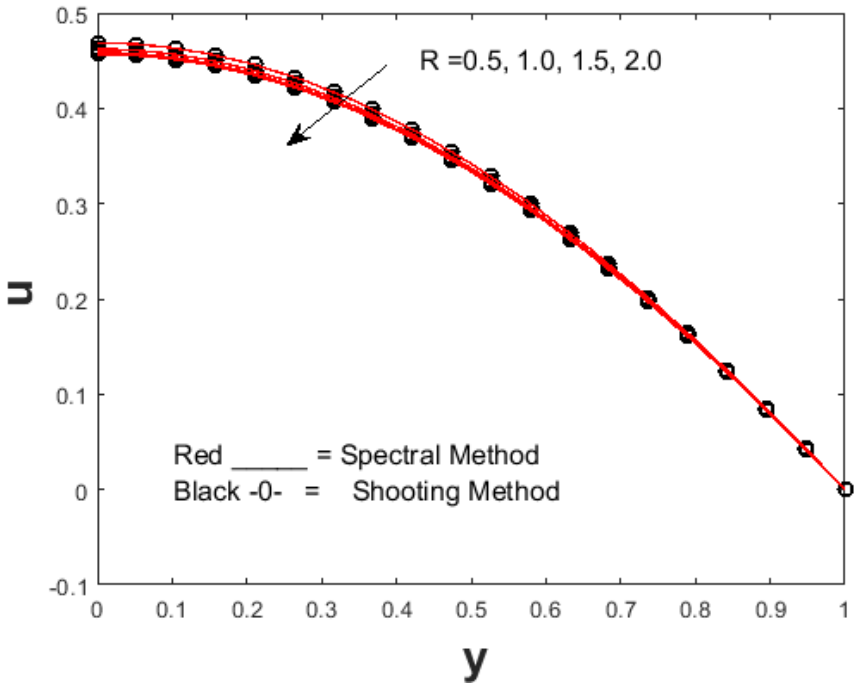

Figure 9: Displacement profiles for different values of *R*

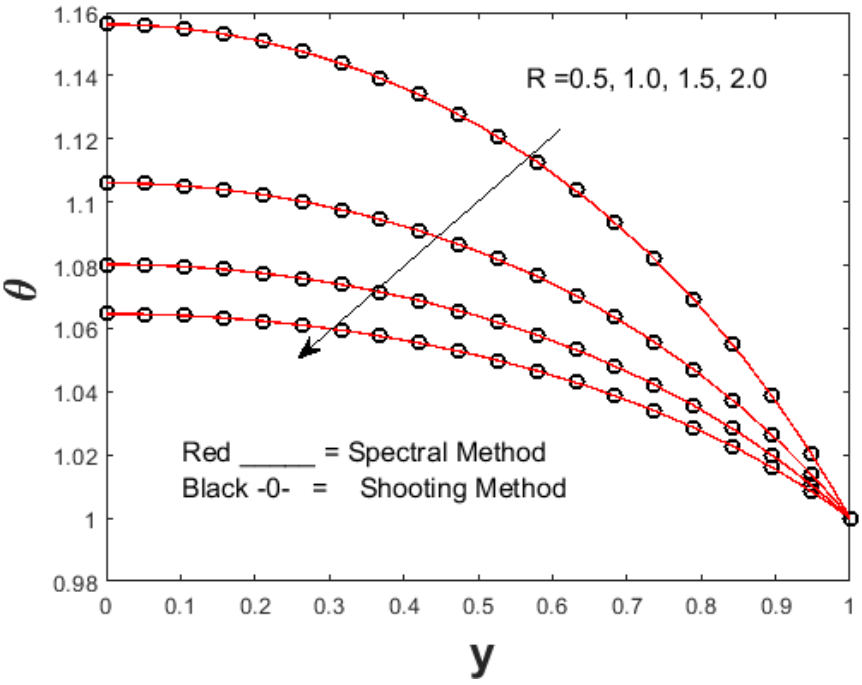

Figure 10: Temperature profiles for different values of *R*

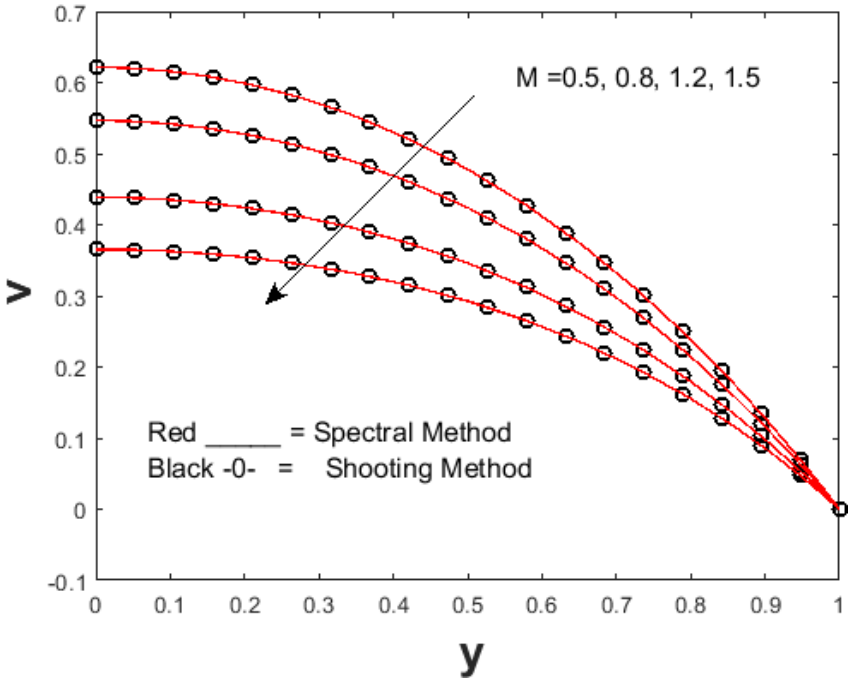

Figure 11: Velocity profiles for different values of *M*

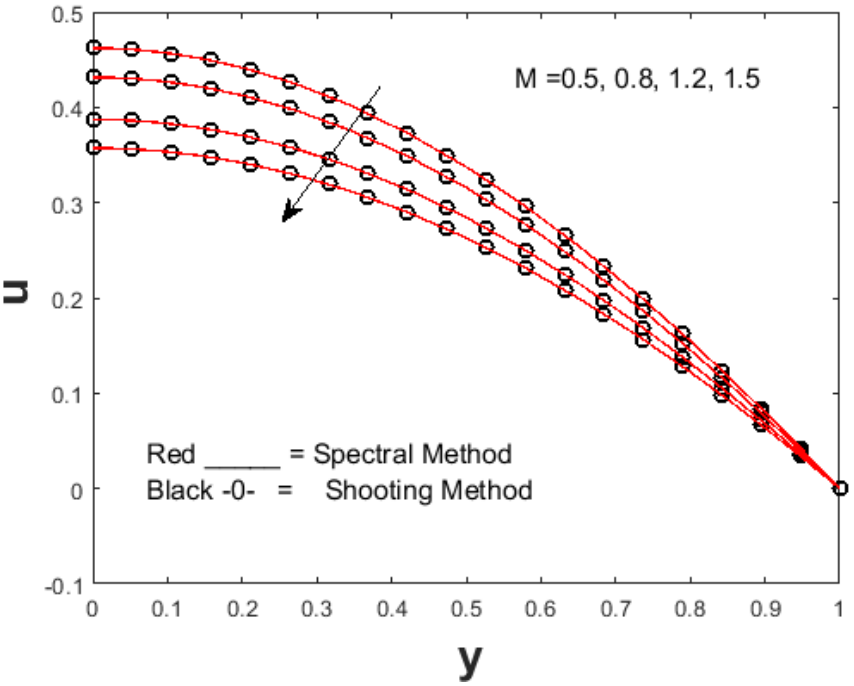

Figure 12: Displacement profiles for different values of *M*

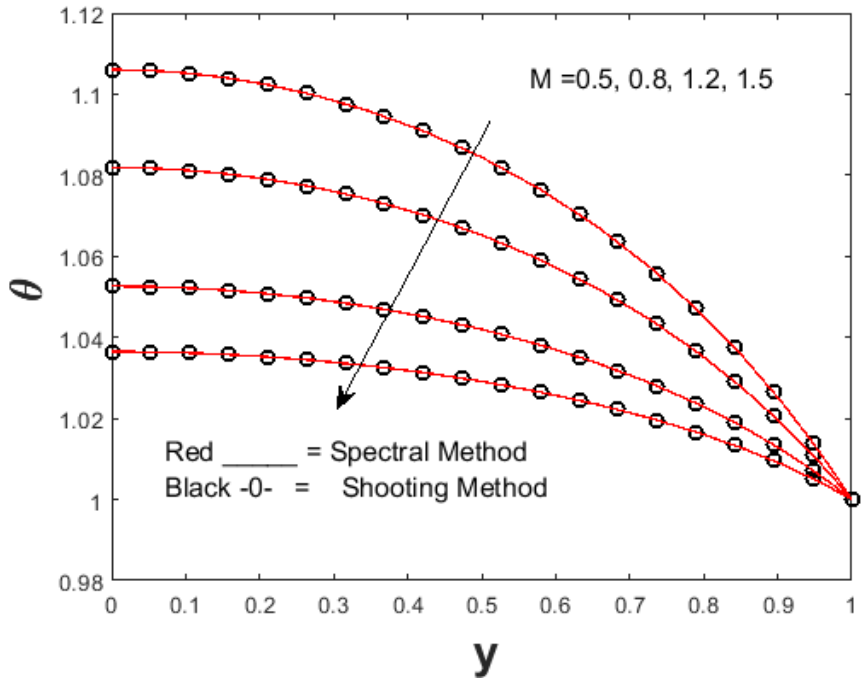

Figure 13: Temperature profiles for different values of *M*

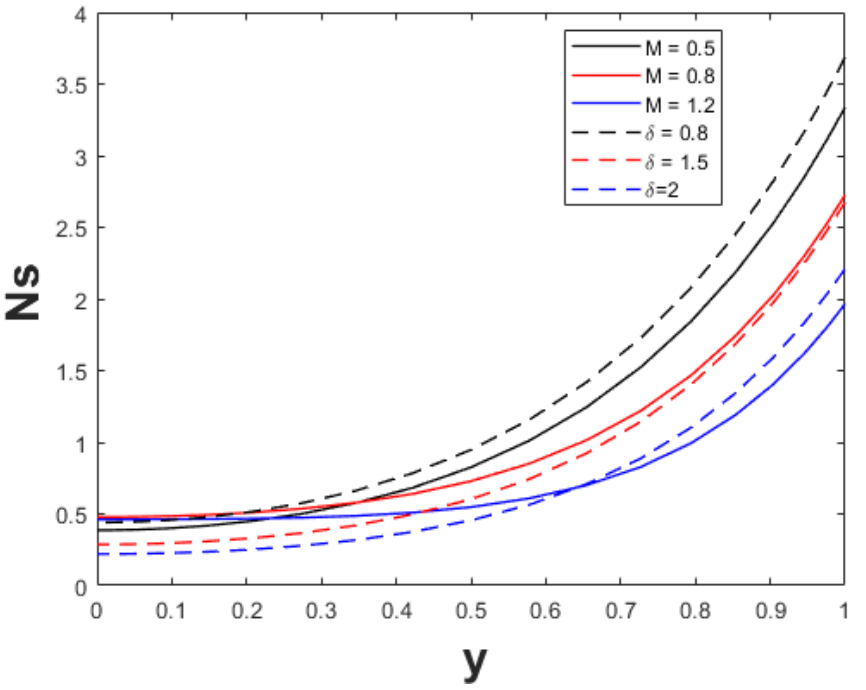

Figure 14: Entropy generation for different of δ and *M*

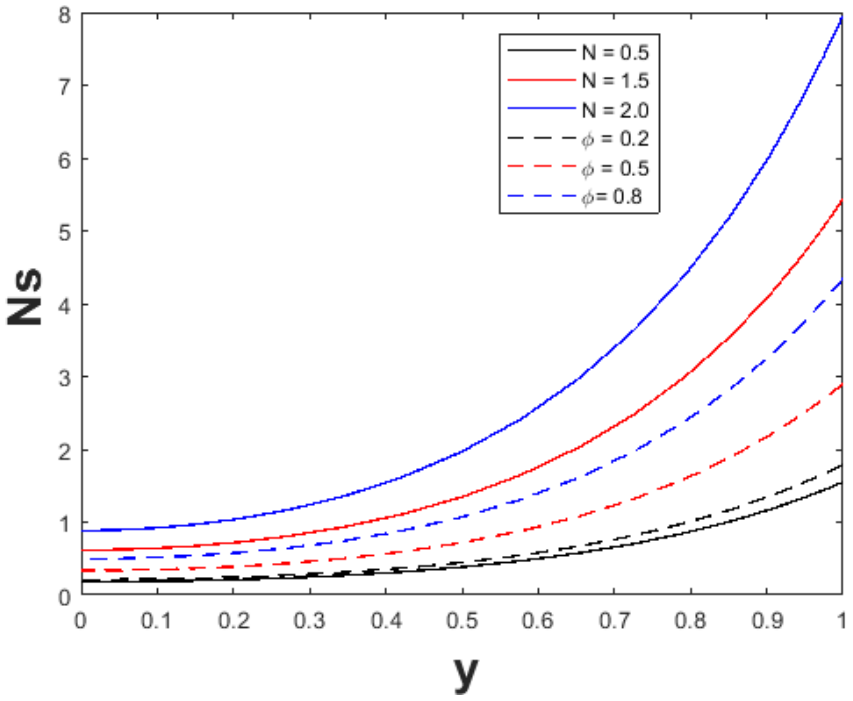

Figure 15: Entropy generation number for different of ϕ and N

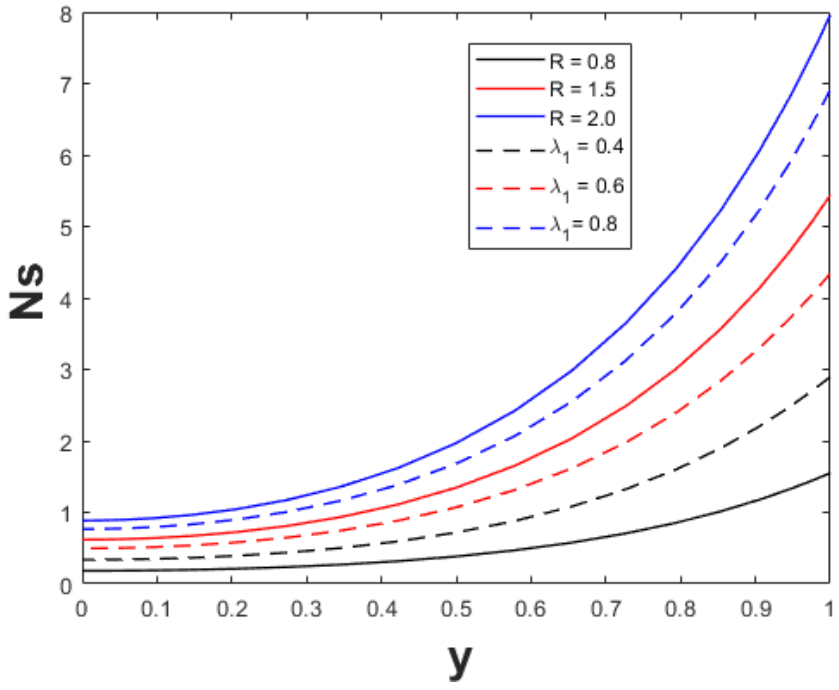

Figure 16: Entropy generation for different values of λ_1 and R

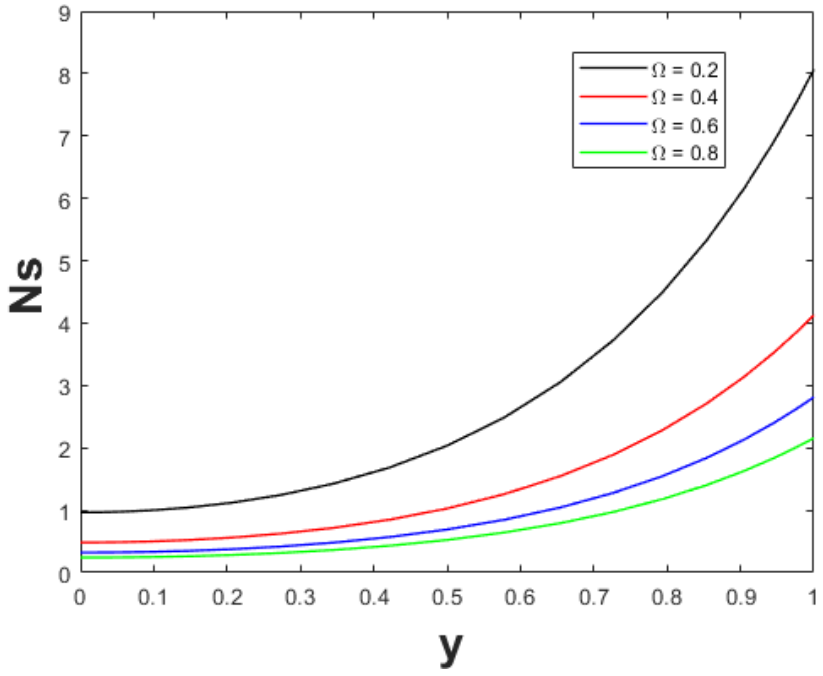

Figure 17: Entropy generation for different values of Ω

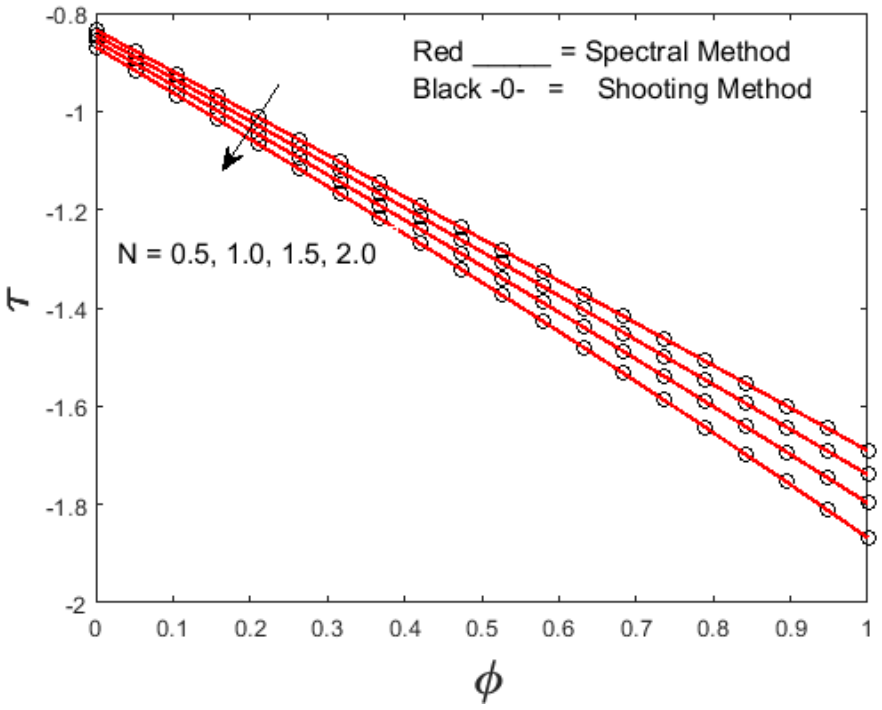

Figure 18: Skin friction as a function of ϕ for different values of N

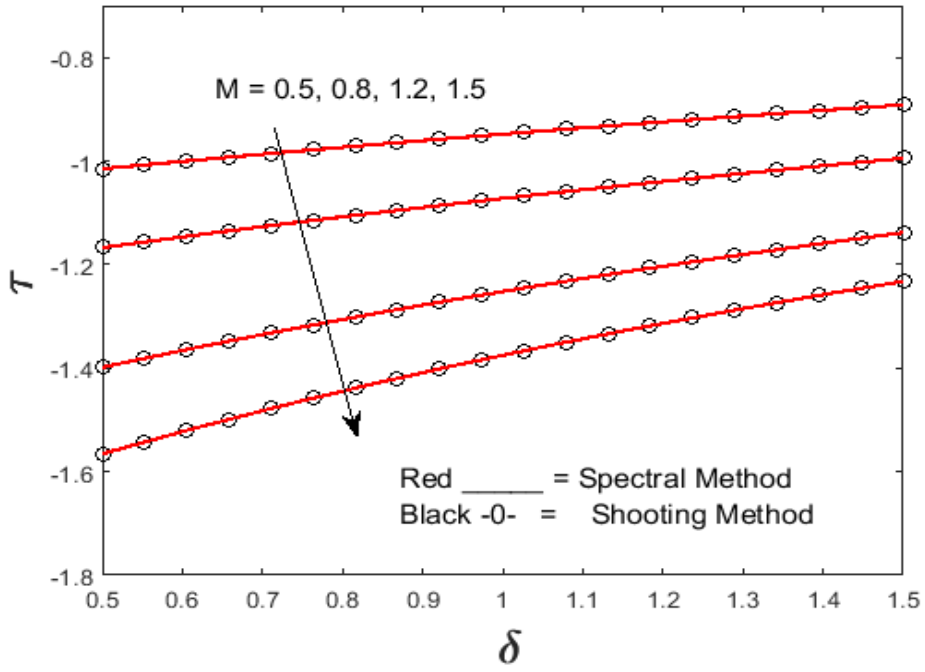

Figure 19: Skin friction as a function of δ for different values of M

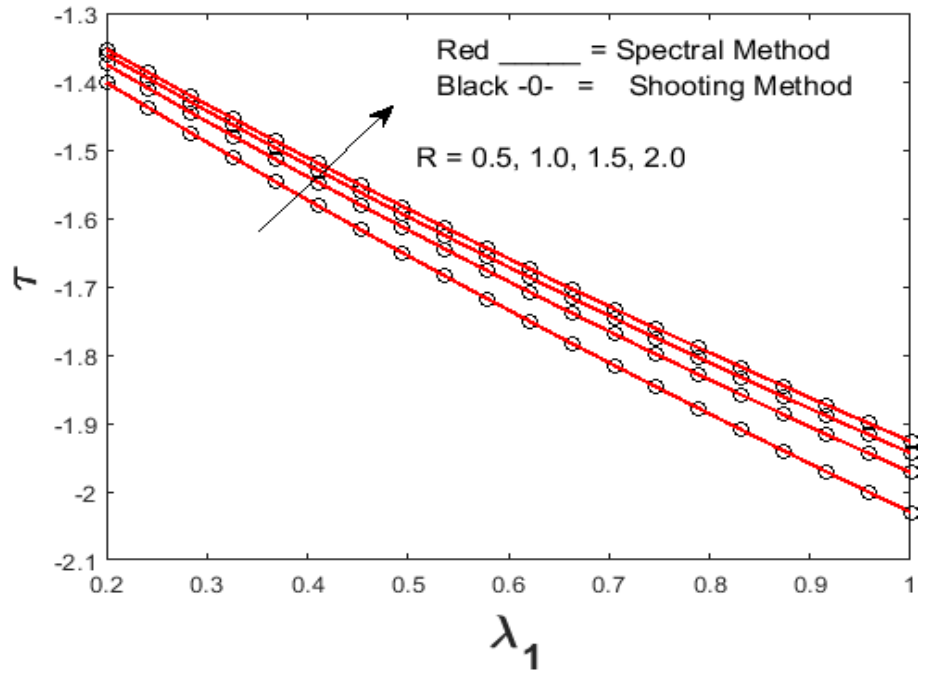

Figure 20: Skin friction as a function of λ_1 for variation of R

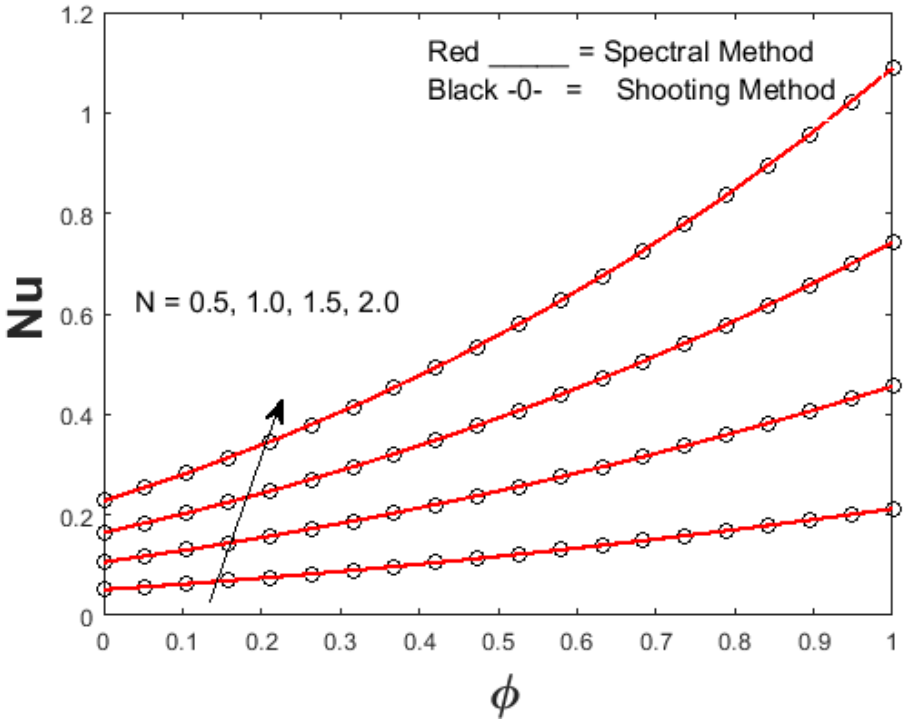

Figure 21: Nusselt number as function of ϕ for different values of N

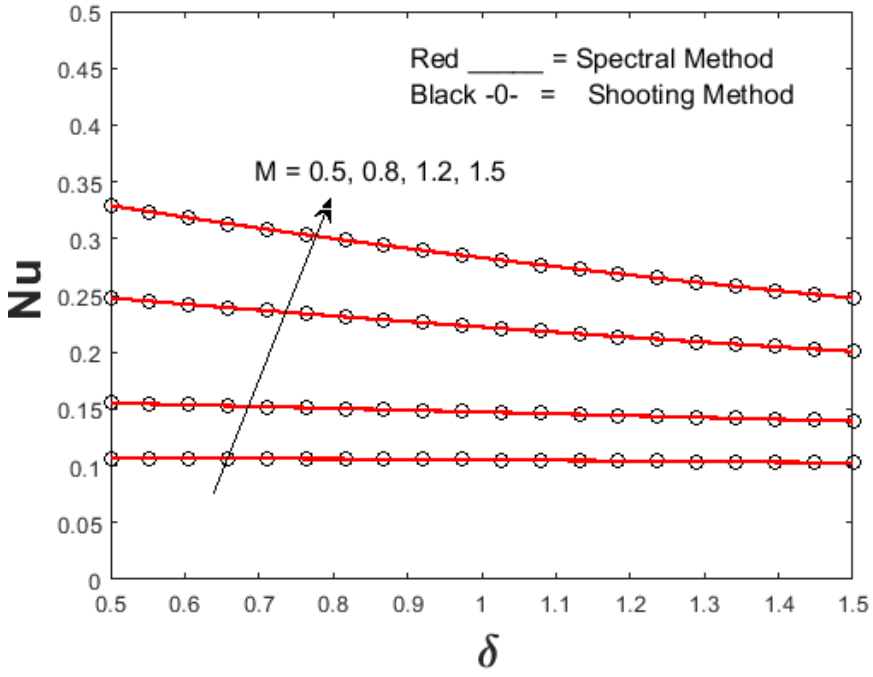

Figure 22: Nusselt number as a function of δ for different values of M

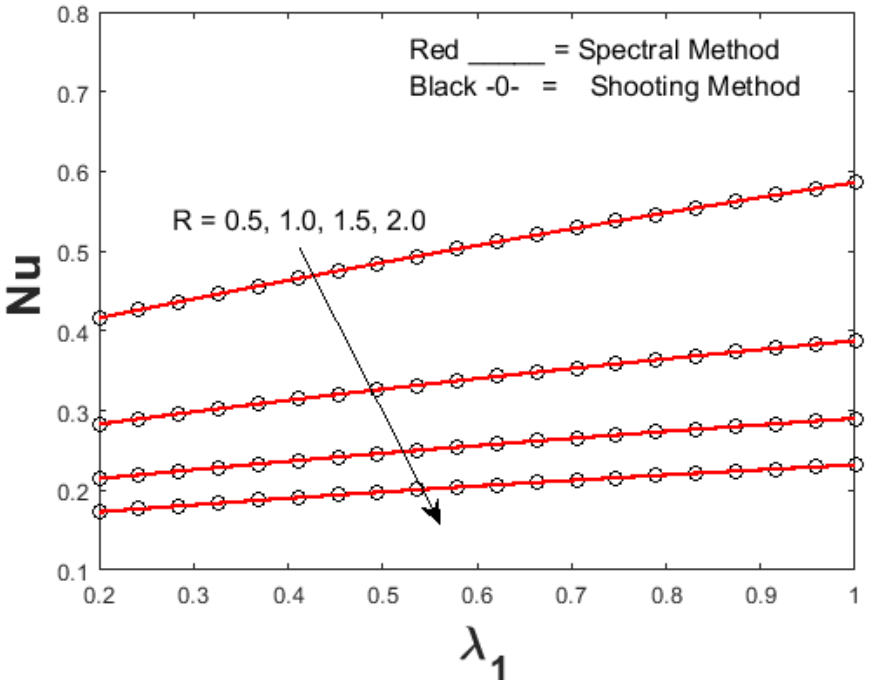

Figure 23: Nusselt number as a function of λ_1 for different values of R

Nusselt number, *Nu* i.e. dimensionless heat transfer gradient at the wall is given by:

$$Nu = -[d\theta/dy]_{y=1} \quad (35)$$

It is also note-worthy that only the right hand channel half-space is studied since the system is symmetrical about the channel centre-line i.e. all computations are presented for the range $0 \leq y \leq 1$. Additionally we note that in all graphs both SQM and shooting numerical quadrature solutions have been presented and achieve excellent agreement. Confidence in the SQM code utilized is therefore justifiably high.

Figs. 5-7 illustrate the velocity (v), solid displacement (u) and temperature (θ) distributions for different values of viscous drag parameter (δ). This parameter embodies the Darcian matrix resistance i.e. impedance to which it is directly proportional i.e. $\delta = Kh^2/(2\mu_a)$. It features in the normalized elastic equilibrium (6) and energy conservation (10) equations as a positive linear and quadratic body force terms in terms of flow velocity i.e. $+\delta v$ *and* $+N\delta v^2$, *respectively*. However it appears as a negative body force in the momentum conservation eqn. (7), viz $-\delta v$. The inhibitive nature of this porous media drag force leads to a significant deceleration in fluid flow, as observed in Fig. 5. Increasing values of K and

therefore δ, imply an accentuation in the impedance offered by the porous media solid fibers to percolating flow. Consistently maximum fluid velocity is computed at the centreline and vanishes at the channel wall (right hand side plate) in consistency with the no-slip boundary condition imposed there. Conversely with larger values of δ, solid displacement is enhanced across the channel half-space region in Fig. 6. The increase retardation of the biofluid manifests in an elevation in poro-elastic stress generated between the porous media fibers. The deformability of the medium permits these stresses to generate significant displacements characteristic of poro-elastic materials, via inter-pore fluid pressure as noted by Coussy [1], Liu *et al.* [58] and Cheng and Detorunay [59]. Temperature however is strongly reduced with increasing viscous drag parameter, as plotted in Fig. 7. The buoyancy force $+N\delta v^2$, in Eqn. (10) encourage momentum diffusion in the regime. However it reduces thermal convection which leads to a depletion in temperatures across the channel half-space. Stronger viscous drag associated with the poro-elastic medium therefore effectively cools the regime and this has important implications in biothermal therapy procedures.

Figs. 8-10 depict the evolution in fluid velocity, solid displacement and temperature distribution across the channel half space with variation in radiation-conduction parameter, R. This parameter defines the relative contribution of thermal radiation heat transfer to thermal conduction heat transfer. It only features in the augmented thermal diffusion term in the normalized energy eqn. (10) i.e. it is absent from the elastic equilibrium and momentum conservation equations although via coupling it does exert an indirect effect on displacement and velocity. When $R < 1$ thermal radiation dominates over thermal conduction, for $R > 1$ thermal conduction dominates. When $R = 1$ both thermal conduction and thermal radiation contributions are equal . Increasing R value i.e. decreasing thermal radiation is found to elevate fluid velocity (v) as seen in Fig. 8. Increasing radiative flux is known to energize fluids and simultaneously supplies supplementary energy to the velocity field i.e. induces acceleration, as noted by Srinivas *et al.* [24], Shukla *et al.* [26] and also Cess [60]. The radiation interacts in a complex manner with both thermal convection and thermal conduction. The maximum effect is sustained at the channel centre-line and decays with proximity to the channel plate (wall). Fig. 9 indicates that the displacement field is also weakly suppressed with a rise in R values i.e. displacments are increased with radiative heat flux. Stress state of the poro-elastic medium is therefore elevated by thermal radiation. This has significant benefit in for example high intensity focused ultrasound (HIFU) ablation

treatments where strong thermal fields contribute to enhanced local tissue movement, as noted by Wang [61]. Fig. 10 illustrates that temperatures are much more significantly boosted with a decrease in R values. Significant energization of the biofluid is achieved with $R < 1$ whereas cooling is induced with $R > 1$. The profiles are substantially modified as compared with displacement and velocity field which are marginally influenced.

Figs. 11-13 illustrate the impact of magnetic body force parameter on fluid velocity, solid displacement and temperature distributions. Velocity of the fluid decreases when the magnetic parameter (*M)* increases. Higher values of *M* correspond to stronger external magnetic field. This in turn accentuates the Lorentzian drag force (generated due to an interaction between the magnetic field induction and electric current density) which increases the impedance to the flow i.e. induces retardation and a reduction in fluid velocity magnitudes. When $M < 1$ the viscous hydrodynamic force exceeds the hydromagnetic drag force and vice versa for $M > 1$. Despite the marked deceleration in flow there is never any back flow induced or flow separation. The flow remains stable across the channel half-space. Evidently the flow is strongly regulated by the action of a magnetic field and this is of significance in magnetic thermal therapy procedures including biomagnetic regulation of blood flow in vascular tissue [15]. Displacements are also considerably reduced with greater magnetic field effect, as observed in Fig. 12. However the reduction is significantly lower for the velocity field. Although magnetic field does not feature in the elastic equilibrium eqn. (6), via poro-elasticity the damping in the velocity field leads to a modification in pressure distribution and this influences the displacement field. Although this effect is more prominent in anisotropic porous media, it still exerts some contribution in the isotropic model under consideration. Modeling poroelasticity requires the coupling of two laws, namely *Darcy's law* and the *structural displacement law for the porous matrix*. Darcy's law describes the relation between fluid motion and pressure within a porous medium and implies that fluid velocity is directly proportional to the difference in pressure over a given distance and the fluid's viscous properties and the porous material's ability to disrupt the flow . The structural displacement of the porous matrix relates to elastic equilibrium and the *Biot poroelasticity approach* successfully describes this coupled physics and is utilized in the current model. Temperatures are also strongly depressed with increasing magnetic field parameter, as visualized in Fig. 13. This behaviour deviates from the classical result in viscous magnetohydrodynamics in non-deformable porous media. Generally when the

medium cannot deform, the supplementary work expended in dragging the fluid against the action of the applied magnetic field is dissipated as thermal energy . This heats the medium. However in poro-elastic media, since deformation is possible, the displacement field allows a modification in the porous matrix structure which manifests in a cooling effect with increasing magnetic field. This has been noted by several investigators including Boopalan [62] and is beneficial to both tissue and cartilage repair.

Figs. 14-17 depict the effects of magnetic parameter M, drag parameter δ, buoyancy parameter N, fluid fraction ϕ, radiation-conduction parameter R, Jeffrey parameter λ_1 and temperature difference parameter, Ω, on the entropy generation number N_s. In this study, as noted earlier, we have selected the following default values for the numerical computations: $P=-1,\ \phi=0.6,\ \delta=1,\ N/\Omega=1,\ \mathrm{R}=1,\ N=1,\ \lambda_1=0.2,\ M=1$. Fig. 14 presents the evolution in entropy generation number N_s across the channel half-space for different values of M and δ. It is noticed that magnetic field induces a considerable reduction in entropy generation. This is attributable to the strong damping in velocity field with greater magnetic field. This behaviour has also been observed by other researchers including Khan *et al*. [22] and Vyas and Srivastava [57]. It is also evident that entropy generation number decreases significantly with increasing viscous drag (porous impedance) parameter δ since again this is associated with strong retardation of the flow. This implies that the parameters M and δ can successfully control the entropy production in the channel, confirming the advantage of using magnetic therapy from a thermodynamic optimization viewpoint. Fig. 15 shows that "entropy generation number decreases with increasing buoyancy parameter N and volume fraction of the fluid ϕ. Thermal buoyancy is associated with flow deceleration in natural convection regimes. Velocity is reduced and this leads to a suppression in entropy generation. In poro-elasticity, the application of any external load to the deformable porous medium modifies the volume fraction of the pores. The fluid-filled pores experience a change in pressure under this mechanical stress, which, in turn, generates fluid motion. As a reaction to this change in pore volume, the solid material shifts and deforms elastically". Increasing volume fraction produces lower flow velocities which result in a decrease in entropy generation. Maximum modifications are consistently computed at the channel plate (wall). Entropy generation is observed to grow from the channel centre-line to the channel boundary since velocity is reduced over this same range (velocity vanishes at the wall).

Fig. 16 illustrates the variation in the entropy generation number with radiation-conduction parameter R and Jeffrey parameter λ_1. It is seen that an increase in Jefferys viscoelastic parameter mobilizes a significant elevation in entropy generation. This parameter denotes the ratio of the relaxation to retardation times of the biofluid. When $\lambda_1 = 1$, *both relaxation and retardation time are exactly equivalent.* However, in the context of biological media, it is more appropriate to consider $\lambda_1 < 1$ for which retardation time exceeds the relaxation time. It is also interesting to note that whereas both the viscosity and elasticity vary greatly among the pathological fluids, the elasticity is the more sensitive indicator of viscoelastic properties. This implies that the biofluid responds faster with the removal of stress and returns quicker to its unperturbed state. This influences pressure gradient and" elevates the velocity field since elastic forces are accentuated and viscous effects are reduced progressively with larger values of λ_1. The acceleration in the flow leads to an enhancement in entropy generation. An increase in R value (decrease in radiative heat transfer contribution) is also observed to lead to an escalation in entropy generation number, N_s. Both viscoelasticity and radiative flux are therefore counter-productive in terms of thermodynamic optimization of the biological system. Inspection of Fig. 17 shows that there is a dramatic depression in entropy generation across the channel half space with increasing temperature difference parameter (Ω) values. Eqn. (32) i.e. $N_s = \left[1+\frac{4}{3}R\right]\left(\frac{d\theta}{dy}\right)^2 + \frac{N}{\Omega}\left[\left(\frac{dv}{dy}\right)^2 + Mv^2\right]$ clearly shows the inverse relationship between N_s. Larger temperature differences lead to a stabilization in thermal convection and inhibit entropy generation, as noted by Vasu *et al*. [16] and Akbar *et al*. [18]. The impact as noted earlier is amplified at the channel wall and minimized at the central (core) zone of the channel. As with other plots (Figs 14-16) there is a monotonic increase in entropy generation rate across the channel half space.

Figs. 18-20 visualize the effects of buoyancy parameter (N), magnetic body force parameter (M), and thermal radiation-conduction parameter (R) on skin friction at the right hand channel plate (y =1) as function of ϕ, δ, and λ_1, respectively. It is observed that the skin friction decreases with buoyancy and magnetic parameters (since velocity fields are reduced) whereas the opposite behaviour is noticed in the case of radiation-conduction parameter. Skin friction is also observed in Fig 18 to be depressed in a linear fashion with

increasing volume fraction. However it grows significantly with increasing viscous drag parameter (Fig. 19) but is again strongly reduced with greater Jefferys viscoelastic parameter (Fig. 20). These trends are intimately connected with the influence of the same parameters on the velocity field described in earlier graphs.

Figs. 21-23 present the evolution in Nusselt number and presented through Figs. 20-23. It is pointed out that the Nusselt number increases with respect to buoyancy and magnetic parameters since *greater heat transfer to the wall* is achieved with a reduction in temperatures. However Nusselt numbers are noticeably suppressed with increasing R values since temperatures are decreased and this augments heat diffusion rates from the biofluid to the channel plate. These trends concur with the earlier study of Hidouri *et al.* [63] which indicates that radiation effect homogenizes the temperature inside the channel by decreasing the temperature gap between the two insulated channel walls, resulting in depletion in Nusselt numbers.

6. CONCLUSIONS

Motivated by providing a multi-physical model of transport in deformable magneto-biothermal systems, a mathematical and numerical study has been presented in this article, for *magnetohydrodynamic biological flow, heat transfer and entropy generation in electro-conductive viscoelastic flow in a vertical channel containing a poro-elastic medium*. Thermal buoyancy and radiative flux effects have been included. The non-dimensionalized boundary value problem has been solved numerically to yield robust solutions for fluid velocity, solid displacement and temperature distribution. Additionally solutions for entropy generation rate, wall shear stress at the right hand plate and Nusselt number have been presented. Verification of the accuracy of the SQM computations has been achieved with an alternate numerical method i.e. shooting quadrature. The effects of various physical parameters on fluid velocity, solid displacement, temperature, entropy generation, shear stress and Nusselt numbers have been visualized graphically. The present simulations have shown that

(i) Increasing viscous drag (porous media impedance) parameter decreases the fluid velocity.
(ii) Increasing magnetic force and drag parameters decrease both velocity and entropy production rates.

(iii) Entropy production is enhanced with an increase in thermal buoyancy parameter and volume fraction of the fluid.

(iv) Skin friction decreases with elevation in thermal buoyancy and magnetic body force parameter whereas the reverse trend is computed with increasing radiation-conduction parameter.

(v) Nusselt number increases with an increase in thermal buoyancy and magnetic body force parameter whereas the converse behaviour is induced with increasing values of radiation-conduction parameter .

(vi) Skin friction is strongly reduced with increasing viscoelastic parameter whereas Nusselt number is elevated.

(vii) Elastic displacement in the deformable porous medium is boosted with increasing viscous drag parameter, whereas it is weakly decreased with increasing radiation-conduction parameter and strongly reduced with increasing magnetic body force parameter .

(viii) The case for a viscous Newtonian fluid can be retrieved in the present model by taking $\lambda_1 \to 0$ and $\lambda_2 \to 0$.

REFERENCES

[1] O. Coussy, *Mechanics of Porous Continua*, Wiley, New York (1995).

[2] Biot, M.A., General theory of three-dimensional consolidation, *J. Appl. Phys*, 12(2) (1941) 155-164.

[3] V.C. Mow, M.H. Holmest, W.M. Lai, Fluid transport and mechanical properties of articular cartilage: a review, *J. Biomech.*, 17(5) (1984) 377-394.

[4] W.M. Lai, J.S. Hou, V.C. Mow, A triphasic theory for the swelling and deformation behaviors of articular cartilage, *ASME J. Biomech. Eng*., 131 (1991) 245-258.

[5] S.I. Barry, K.H. Parker, G.K. Aldis, Fluid flow over a thin deformable porous layer, *ZAMP- J. Appl. Math. Phy*., 42 (1991) 633-648.

[6] S. Sreenadh, K.V. Prasad, H. Vaidya, E. Sudhakara, G. Gopi Krishna, M. Krishnamurthy, MHD Couette flow of a Jeffrey fluid over a deformable porous layer, *Int. J. Appl. Comput. Math.*, 3(3) (2017) 2125--2138.

[7] Sreenadh, S., Rashidi, M.M., Kumara Swami Naidu, K. and Parandhama, A., Free convection flow of a Jeffrey fluid through a vertical deformable porous stratum, *J. Appl. Fluid Mech.*, 9(5) (2015) 2391--2401.

[8] M. I. A. Othman, K. Lotfy, S.M. Said, **O. Anwar Bég**, Wave propagation in a fiber-reinforced micropolar thermoelastic medium with voids using three models, *Int. J. Appl. Math. Mech.*, 8(12) (2012) 52-69.

[9] Li-Na Yu and Jing Liu, Entropy generation theory for characterizing the freezing and thawing injury of biological materials, *Forschung im Ingenieurwesen*, 71 (2007) 125.

[10] U. Lucia, Entropy generation approach to cell systems, *Physica A: Statistical Mechanics and its Applications*, 406 (2014) 1-11.

[11] F. Liao, G. L. Y. Cheing, W. Ren, S. Jain, Y.K. Jan, Application of multiscale entropy in assessing plantar skin blood flow dynamics in diabetics with peripheral neuropathy, *Entropy*, *20*(2) (2018) 127.

[12] U. Lucia, A. Ponzetto, T. S. Deisboeck, A thermodynamic approach to the 'mitosis/apoptosis' ratio in cancer, *Physica A: Statistical Mech. its Appl.*, 436 (2015) 246-255.

[13] Miguel, A.F., Scaling laws and thermodynamic analysis for vascular branching of microvessels, *Int. J. Fluid Mech. Res*., 43 (2016) 390--403.

[14] F. Liao, T. D. Yang, F. L Wu, C. Cao, A. Mohamed, Y.K. Jan, Using multiscale entropy to assess the efficacy of local cooling on reactive hyperemia in people with a spinal cord injury, *Entropy*, 21(1) (2019) 90.

[15] M. Rashid, A. B. Parsa, **O. Anwar Bég**, L. Shamekhi, S.M. Sadri and T. A. Bég, Parametric analysis of entropy generation in magneto-hemodynamic flow in a semi-porous channel with OHAM and DTM, *Applied Bionics Biomech.*, 11(1-2) (2014) 47-60.

[16] B. Vasu, Ch. RamReddy, P. V. S. N. Murthy, R. S. R. Gorla, Entropy generation analysis in nonlinear convection flow of thermally stratified fluid in saturated porous medium with convective boundary condition, *ASME J. Heat Transfer* 139(9), 091701 (10 pages) (2017).

[17] Srinivas, J. and Ramana Murthy, J. V., Second law analysis of the flow of two immiscible micropolar fluids between two porous beds, *J. Eng. Thermophy*., 25(1) (2016) 126-142.

[18] N. S. Akbar, M. Shoaib, D. Tripathi, S. Bhushan and **O. Anwar Bég**, Analytical approach for entropy generation and heat transfer analysis of CNT-nanofluids through ciliated porous medium, *J. Hydrodynamics*, 30(2) (2018) 1-11.

[19] P. Datta, P. S. Mahapatra, K. Ghosh, N. K. Manna, S. Sen, Heat transfer and entropy generation in a porous square enclosure in presence of an adiabatic block, *Transp. Porous Media*, 111 (2016) 305--329.

[20] Rashidi, I., Kolsi, L., Ahmadi, G., Mahian, O., Wongwises, S. and Abu-Nada, E., Three-dimensional modelling of natural convection and entropy generation in a vertical cylinder under heterogeneous heat flux using nanofluids. *International Journal of Numerical Methods for Heat & Fluid Flow*, 30(1), 2019, 119-142.

[21] A. Patronis, R. A. Richardson, S. Schmieschek, B. J. N. Wylie, R. W. Nash, P. V. Coveney, Modeling patient-specific magnetic drug targeting within the intracranial vasculature, *Front. Physiol*., (2018). https://doi.org/10.3389/ fphys. 2018.00331

[22] **O. Anwar Bég**, M.M. Rashidi, N. Kavyani and M.N. Islam, Entropy generation in hydromagnetic convective Von Kármán swirling flow: homotopy analysis, *Int. J. Applied Math. Mech.*, 9(4) (2013) 37-65.

[23] N. S. Khan, Z. Shah, S. Islam, I. Khan, T. A. Alkanhal, I. Tlili, Entropy generation in MHD mixed convection non-Newtonian second-grade nanoliquid thin film flow through a porous medium with chemical reaction and stratification, *Entropy, 21*(2) (2019) 139.

[24] J. V. Ramana Murthy, **O. Anwar Bég**, J. Srinivas, J. V. Ramana Murthy, Entropy generation analysis of radiative heat transfer effects on channel flow of two immiscible couple stress fluids, *J. Brazilian Soc. Mech. Sci. Eng.*, 39 (2017) 2191-2202.

[25] Srinivas, J., Adesanya, S. O., Falade, J. A. and Nagaraju, G., Entropy generation analysis for a radiative micropolar fluid flow through a vertical channel saturated with non-Darcian porous medium, *Int. J. Appl. Comput. Math*., 3(4) (2017) 3759-3782.

[26] M. Y. A. Jamalabadi, P. Hooshmand, A. Hesabi, M. K. Kwak, I. Pirzadeh, A. J. Keikha, M. Negahdari, Numerical investigation of thermal radiation and viscous effects on entropy generation in forced convection blood flow over an axisymmetric stretching sheet, *Entropy*, 18(6) (2016) 203.

[27] N. Shukla, P. Rana, **O. Anwar Bég**, **A. Kadir**, B. Singh, Unsteady electromagnetic radiative nanofluid stagnation-point flow from a stretching sheet with chemically reactive nanoparticles, Stefan blowing effect and entropy generation, *Proc. I Mech E: Part N- J. Nanomaterials, Nanoeng. Nanosystems.*, (2018). *DOI: 10.1177/2397791418782030 (14 pages).*

[28] Muthukumar, S., Sureshkumar, S., Chamkha, A.J., Muthtamilselvan, M. and Prem, E., 2019. Combined MHD convection and thermal radiation of nanofluid in a lid-driven porous enclosure with irregular thermal source on vertical sidewalls. *Journal of Thermal Analysis and Calorimetry*, 138(1), pp.583-596.

[29] Li, Z., Sheikholeslami, M., Chamkha, A.J., Raizah, Z.A. and Saleem, S., 2018. Control volume finite element method for nanofluid MHD natural convective flow inside a sinusoidal annulus under the impact of thermal radiation. *Computer Methods in Applied Mechanics and Engineering*, 338, pp.618-633.

[30] L. Campo-Deaño, Viscoelasticity of blood and viscoelastic blood analogues for use in polydymethylsiloxane in vitro models of the circulatory system, *Biomicrofluidics*, 7(3) (2013) 034102.

[31] G. B. Thurston, H. Greiling, Viscoelastic properties of pathological synovial fluids for a wide range of oscillatory shear rates and frequencies, *Rheologica Acta*, 17 (1978) 433--445.

[32] A. F. Silva, M. A. Alves, Mónica S. N. Oliveira, Rheological behavior of vitreous humour, *Rheologica Acta*, 56 (2017) 377-386.

[33] R. Hirose, T. Nakaya, Y. Naito, T. Daidoji, O. Dohi, N. Yoshida, H. Yasuda, H. Konishi, Y. Itoh, Identification of the critical viscoelastic factor in the performance of submucosal injection materials, *Materials Sci. Eng.: C*, 94 (2019) 909-919.

[34] WA van der Reijden, EC Veerman, AV Amerongen, Shear rate dependent viscoelastic behavior of human glandular salivas, *Biorheo.*, 30(2) (1993) 141--152.

[35] A. Zaman, N. Ali, **O. Anwar Bég** and M. Sajid, Heat and mass transfer to blood flowing through a tapered overlapping stenosed artery, *Int. J. Heat Mass Trans.*, 95 (2015) 1084-1095.

[36] S.O. Adesanya, J.A. Falade, J. Srinivas, **O. Anwar Bég**, Irreversibility analysis for reactive third-grade fluid flow and heat transfer with convective wall cooling, *Alexandria Eng. J.*, 56 (2017) 153-160.

[37] M. Kumar, G. J. Reddy, G. Ravi Kiran, M.A.M. Aslam, **O. Anwar Bég**, Computation of entropy generation in dissipative transient natural convective viscoelastic flow, *Heat Transfer Asian Research*, 1-26 (2019). DOI: 10.1002/htj.21421.

[38] K. Vajravelu, S. Sreenadh, L. Lakshminarayana, The influence of heat transfer on peristaltic transport of a Jeffrey fluid in a vertical porous stratum, *Commun. Nonlinear Sci. Numer. Simulation*, 16 (2011) 3107-25.

[39] D. Tripathi, **O. Anwar Bég**, Mathematical modelling of heat transfer effects on swallowing dynamics of viscoelastic food bolus through the human oesophagus, *Int. J. Therm. Sci.*, 70 (2013) 41-53.

[40] Yu. M. Chernyakova, L. S. Pinchuk, L. S. Lobanovskii, E. S. Drozd, S. A. Chizhik, Structure and magnetic susceptibility of lubricating fluids in synovial joints, *J. Friction Wear*, 32(1) (2011) 54--60.

[41] CH Liu, WC Wu, HY Lai, HY Hou, Magnetic purification of plasminogen from human plasma by specific lysine affinity, *J. Biosci. Bioeng.*, 112(3) (2011) 219-224.

[42] P.A. Voltairas, D.I. Fotiadis, L.K. Michalis, Hydrodynamics of magnetic drug targeting, *J. Biomech.*, 35(6) (2002) 813-21.

[43] B. Shapiro, S. Kulkarni, A. Nacev, A. Sarwar, D. Preciado, D.A. Depireux, Shaping magnetic fields to direct therapy to ears and eyes, *Ann. Rev. Biomed. Eng.*, 16 (2014) 455-481.

[44] N. Manzoor, K. Maqbool, **O. Anwar Bég**, S. Shaheen, Adomian decomposition solution for propulsion of dissipative magnetic Jeffrey biofluid in a ciliated channel containing a porous medium with forced convection heat transfer, *Heat Transfer*, 1-26 (2018). DOI: 10.1002/htj.21394

[45] K. Ramesh, D. Tripathi, **O. Anwar Bég**, **A. Kadir**, Slip and Hall current effects on viscoelastic fluid-particle suspension flow in a peristaltic hydromagnetic blood micropump, *Iranian J. Science Tech. Trans. Mech. Eng*. (2018). doi.org/10.1007/s40997-018-0230-5

[46] G. Gopi Krishna, S. Sreenadh, A.N.S. Srinivas, Entropy generation and heat transfer in a Casson fluid flow through a vertical deformable porous stratum, *World Appl. Sci. J.*, 35(7) (2017) 1059-1067.

[47] G. Gopi Krishna, S. Sreenadh, A.N.S. Srinivas, An entropy generation on viscous fluid in the inclined deformable porous medium, *Differ. Equ. Dyn. Syst*., (2018). DOI: 10.1007/s12591-018-0411-0

[45] R. Bellman, R. Kalaba, *Quasilinearization and Nonlinear Boundary Value Problems*, Elsevier, USA (1965).

[46] B. Mallikarjuna, A.M.Rashad, Ali.J. Chamkha and S. Hariprasad Raju, Chemical reaction effects on MHD convective heat and mass transfer flow past a rotating vertical cone embedded in a variable porosity regime, *Afrika Matematika*, 27(3-4), (2016), 645-665.

[47] S. Sreenadh, G. Gopi Krishna, A.N.S Srinivas, E. Sudhakara, Entropy generation analysis for MHD flow through a vertical deformable porous layer, *J. Porous Media*, 21(6) (2018) 523-538.

[48] M.Q. Brewster, *Thermal Radiative Transfer and Properties*, Wiley, USA (1992).

[49] L.N.Trefethan, *Spectral methods in MATLAB*, SIAM, Philadelphia, USA (2000).

[50] **O. Anwar Bég**, S.S. Motsa, M.N. Islam, M. Lockwood, Pseudo-spectral and variational iteration simulation of exothermically-reacting Rivlin-Ericksen viscoelastic flow and heat transfer in a rocket propulsion duct, *Comput. Therm. Sci.*, 6(2) (2014) 91-102.

[51] **O. Anwar Bég**, S.S. Motsa, **A. Kadir**, **T.A. Bég**, M.N. Islam, Spectral quasi-linear numerical simulation of micropolar convective wall plumes in high permeability porous media, *J. Eng. Thermophy.*, 25(4) (2016) 1-24.

[52] A.F. Elsayed, **O. Anwar Bég**, New computational approaches for biophysical heat transfer in tissue under ultrasonic waves: Variational iteration and Chebyschev spectral simulations, *J. Mech. Medicine Biology*, 14(3) (2014) 1450043.1-1450043.17.

[53] **O. Anwar Bég**, M. Hameed, **T.A. Bég**, Chebyschev spectral collocation simulation of nonlinear boundary value problems in electrohydrodynamics, *Int. J. Comput. Methods Eng. Sci. Mech.*, 14 (2013) 104-115.

[54] **O. Anwar Bég**, M.M. Hoque, M. Wahiuzzaman, M. Mahmud, M. Ferdows, Spectral numerical simulation of laminar magneto-physiological Dean flow, *J. Mech. Medicine Biology*, 14(3) (2014) 1450047.1-1450047.18.

[55] B. Mallikarjuna, M. Rashid, S.H. Raju, Influence of nonlinear convection and thermophoresis on heat and mass transfer from a rotating cone to fluid flow in porous medium, *Therm. Sci.*, 21(6B) (2017) 2781-2793.

[56] D. Srinivasacharya, B. Mallikarjuna and R. Bhuvanavijaya, Effects of thermophoresis and variable properties on mixed convection along a vertical wavy surface in a fluid saturated porous medium, *Alexandria Eng. J.*, 55 (2016) 1243-1253.

[57] P. Vyas, N. Srivastava, Entropy analysis of generalized MHD Couette flow inside a composite duct with asymmetric convective cooling, *Arab J. Sci. Eng.*, 40 (2015) 603-614.

[58] C. Liu *et al.*, Theory and analytical solutions to coupled processes of transport and deformation in dual-porosity dual-permeability poro-chemo-electro-elastic media, *ASME J. Appl. Mech.*, 85(11) (2018) 111006 (13 pages).

[59] A.H.D. Cheng, E. Detournay, A direct boundary element method for plane strain

poroelasticity, *Int. J. Numer. Anal. Method. Geomecha.,* 12 (1988) 551-572.

[60] R.D. Cess, The interaction of thermal radiation with conduction and convection heat transfer, *Adv. Heat Transf.*, 1 (1964) 1-50.

[61] H. Wang *et al.,* Thermal ablation monitoring using radiation force induced steady state tissue motion, *J. Acoustical Society America*, 115 (2004) 2412.

[62] P. R. J. V. C. Boopalan, Pulsed electromagnetic field therapy results in healing of full thickness articular cartilage defect, *Int Orthop.,* 35(1) (2011) 143--148.

[63] N. Hidouri, M. Bouabid, M. Magherbi, A. B. Brahim, Effects of radiation heat transfer on entropy generation at thermosolutal convection in a square cavity subjected to a magnetic field, *Entropy,* 13(12) (2011) 1992-2012.